6-4-2018 2:00 PM

Effect of material viscoelasticity on frequency tuning of dielectric elastomer membrane resonators

Liyang Tian, *The University of Western Ontario*

Supervisor: Liying Jiang, *The University of Western Ontario*

A thesis submitted in partial fulfillment of the requirements for the Master of Engineering Science degree in Mechanical and Materials Engineering

Abstract

Dielectric elastomers (DEs) capable of large voltage-induced deformation show promise for applications such as resonators and oscillators. However, the dynamic performance of such vibrational devices is not only strongly affected by the nonlinear electromechanical coupling and material hyperelasticity, but also significantly by the material viscoelasticity. The material viscoelasticity of DEs originates from the highly mobile polymer chains that constitute the polymer networks of the DE. Moreover, due to the multiple viscous polymer subnetworks, DEs possess multiple relaxation processes. Therefore, in order to predict the dynamic performance of DE-based devices, a theoretical model that accounts for the multiple relaxation processes is very essential. In this work, by extending the general modelling framework for finite-deformation viscoelasticity, a new model that accounts for the multiple relaxation times of DEs is proposed to study the in-plane oscillation and frequency tuning of DE membrane resonators. It is found that the failure (electrical breakdown or loss-of-tension) of the DE membrane resonator could be delayed by tailoring the microstructure of the DE. In particular, resonators made of DEs with higher viscosity usually fail earlier with smaller deformation and lower resonant frequency, but they are highly adjustable to achieve similar large deformation. The desirable parameters of the tuneable natural frequency range and voltage safe operation range are also explored. Furthermore, it is more effective to tune up the resonant frequency for such DE membrane resonators. This work can provide guidelines on better predicting the dynamic performance of DE-based vibrational devices, as well as their optimal design.

Keywords

Dielectric elastomer, viscoelasticity, frequency tuning, multiple relaxation, resonator, electromechanical coupling.

Acknowledgments

First and foremost, I would like to thank the Western University and excellent faculty and staffs. I would also like to express my sincere gratitude to my supervisor Professor Jiang for the opportunity to work on this project, for valuable discussions, as well as patient guidance, and colleague Jianyou Zhou for the great help in thesis revision, and colleagues Jia Xue, Xiaotian Yi and Yuanping Li for their help and friendship. Their wisdom has taught me a lot about research and life.

Appreciation is also expressed to the following: Professor Siddiqui, Professor Asokanthan and Professor Klassen, for their valuable advices on the project.

Table of Contents

List of Figures

Nomenclature

(dimensionless when the units are not displayed)

V	voltage
ϕ	electric potential
D	electric displacement
E	electric field
Q	electric charges
ε_0	permittivity of air or vacuum
ε_0	relative dielectric constant
W_s	elastic strain energy density function
G	shear modulus
G^{EQ}	equilibrium shear modulus
G^{NEQ}	non-equilibrium shear modulus
χ	the fraction of the purely elastic ground polymer networks
μ_D	shear viscosity (s^{-1})
τ	viscoelastic relaxation time (s)
J_{lim}	stretching limit of the material
V^*	nominal voltage
E_{EB}	dielectric strength

V_{EB}	electrical breakdown voltage
λ	stretch ratio
F	deformation gradient
F^e	elastic deformation gradient
F^i	viscous deformation gradient
G_f	total free energy
W	Helmholtz free energy density
W^{EQ}	equilibrium Helmholtz free energy density
W^{NEQ}	non-equilibrium Helmholtz free energy density
ρ	density of the material
I	second order identity tensor
I^4	fourth order symmetric identity tensor
γ^{-1}	isotropic rank-four mobility tensor
ω_n	natural frequency
Ω_n	nominal natural frequency

Chapter 1

1 Introduction

1.1 Dielectric elastomers and application

The forefront research in the interdisciplinary area of biology and engineering has been bringing great attention to soft materials. Dielectric elastomers as soft electroactive polymers are being studied to mimic the features of biological life by their voltage-induced or charge-induced deformation (Suo, 2010; Zhao, Hong, and Suo, 2007). Since the material shear moduli of dielectric elastomers are normally only a few KPas, they are very flexible and capable of undergoing large deformation (up to ~500% strain). However, their counterparts, piezoelectric crystals and ceramics with shear moduli of a few GPas, are generally brittle and can only reach less than 1% of strain. Moreover, besides being light in weight and relatively inexpensive, dielectric elastomers also possess high energy density (which is usually more than 8 MJ/m^3, while piezoelectric has about 1 MJ/m^3), making them promising materials for transducers to convert mechanical energy into electrical energy (Saito et al., 2004; Romasanta et al., 2015; Tagarielli, et al., 2012; Treloar, et al., 1944; Shankar et al., 2007; Bar-Cohen, 2004; Pelrine et al., 2000). Due to these unique properties and advantages, DEs have been developed as actuators, sensors, resonators, compliant capacitors and generators, which can be potentially used in soft robotics, medical and biomimetic equipment, energy harvesting systems, and MEMS (Zhou et al. 2015b, 2016a and 2017; Chiang et al., 2012; Ahmadi et al., 2013; Anderson et al., 2010; Chiba et al., 2011; Heydt et al., 2006; Huang et al., 2013; Shian, et al., 2014; Karsten et al., 2013; Kornbluh et al., 2002; Lai et al., 2012; O'Brien et al., 2010; O'Halloran et al., 2008; Carpi et al., 2007 and 2008; Kofod et al., 2003).

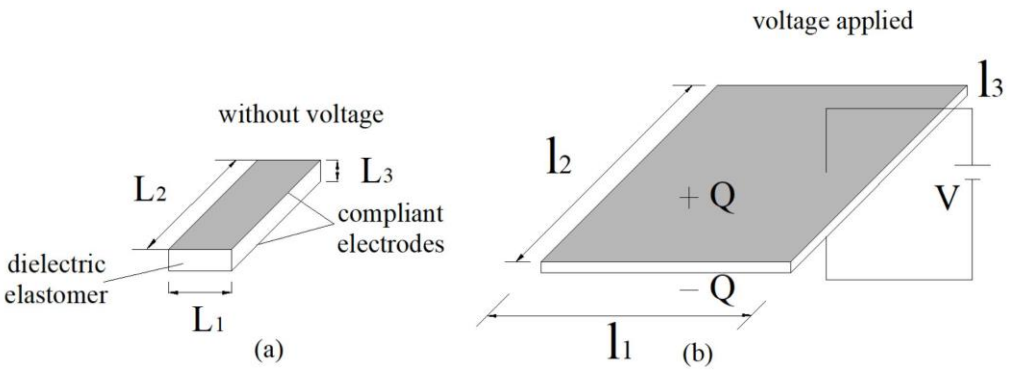

Figure 1.1 Basic schematic of a dielectric elastomer actuator

A typical DE membrane actuator is schematically illustrated in Fig. 1.1. Both surfaces of the DE membrane are coated with highly compliant electrodes, allowing free deformation in three directions of the DE body. When a voltage is applied to the electrodes in Fig. 1.1 (b), an electric field is formed along the thickness direction of the membrane. Meanwhile, the dielectric body is polarized by the induced electric field and the elastomer expands in area and reduces in thickness. The actuator illustrated in Fig. 1.1 can serve as the basic element for more complicated DE-based devices. For example, Figs. 1.2 and 1.3 show some common configurations of DE-based devices in the literature (Kornbluh et al., 2002; Cameron et al., 2008; McKay et al., 2010; Pei et al., 2004; Biggs et al., 2010; Carpi et al., 2007; Pelrine et al., 2002; Ahmadi et al., 2013).

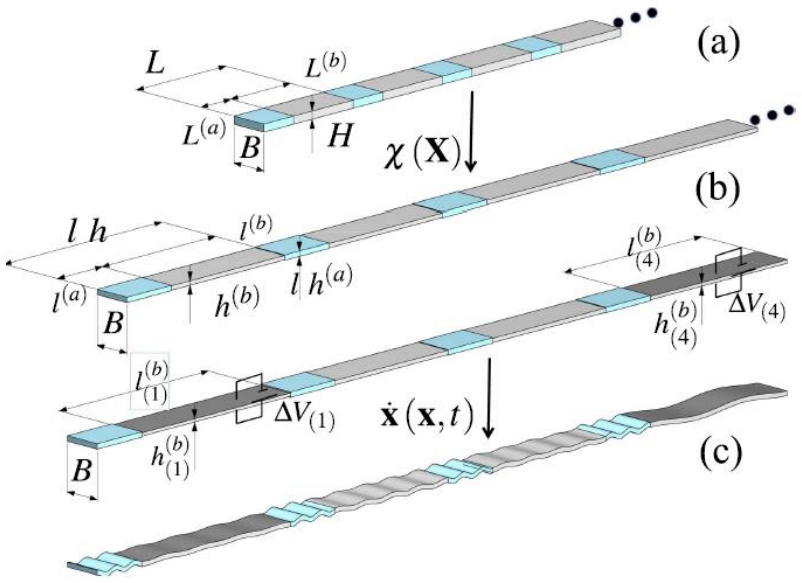

Figure 1.2 Flexural motion manipulation of a four-cell (in grey colour) DE membrane, (a) at the reference state; (b) pre-stretched by the axial tension, while cells 1 and 4 are subjected to $\Delta V_{(1)}$ and $\Delta V_{(2)}$, respectively; (c) with incremental flexural motions superposed on top of static finite deformation (Shmuel et al., 2016).

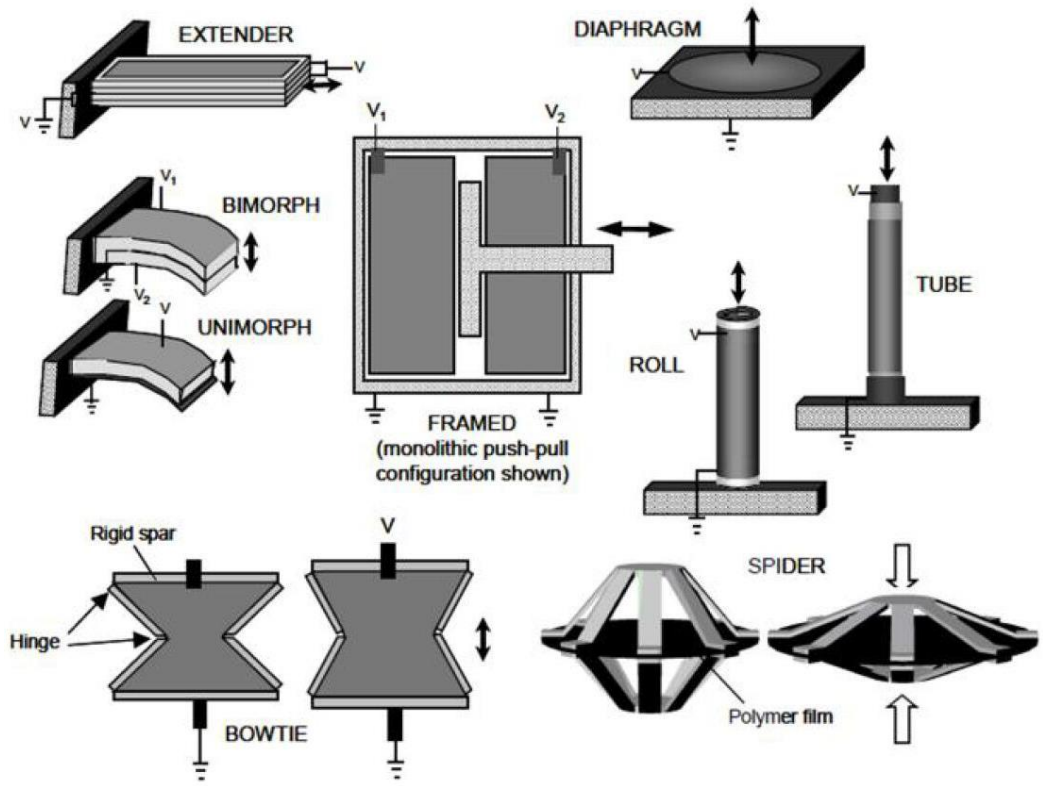

Figure 1.3 Various DE configurations from assembling of membrane elements (Kornbluh *et al.*, 2002).

1.2 Large actuated deformation of dielectric elastomers

The advantage of DE-based devices mainly lies in their large deformation capacity. However, the large deformation of DEs are strongly affected by multiple failure modes such as electrical breakdown and electromechanical instability (Pelrine et al., 1998; Kofod et al., 2003; Plante and Dubowsky, 2006 and 2007; Wissler et al., 2007; Kollosche et al., 2012 and 2015; Koh et al. 2011). The electric breakdown is determined by the electric

strength of the material. When the induced electric field in the DE exceed its dielectric strength, the DE fails by electrical breakdown. The electromechanical instability (EMI) is another significant factor that could limit the large deformation of DEs. When the DE membrane is subjected to a voltage, the reduction in its thickness results in a stronger electric field through the DE membrane even if the applied voltage is fixed, which could lead to an excessive thinning of the DE membrane (electromechanical instability) and premature electrical breakdown (Plante et al., 2006; Keplinger et al., 2012). The interplay between the electromechanical instability and electrical breakdown can be well explained through the electromechanical response curve and electrical breakdown curve of DEs. Actuated by the applied voltage, the electromechanical response of three different types of DEs are shown in Fig. 1.4 (Koh et al., 2011; Zhao et al., 2010; Huang et al., 2011; Leng et al., 2009). As shown in Fig. 1.4(a), DEs with low dielectric strength fails by electrical breakdown with relatively small stretch and the membrane does not undergo EMI. For DEs with moderate dielectric strength, as shown in Fig. 1.4(b), EMI occurs during their actuation and the DE fails by premature electrical breakdown. If the dielectric strength of a DE is high enough, as shown in Fig. 1.4(c), the DE undergoes a snap-through deformation and survive the EMI, and large deformation is achieved. The snap-through deformation is represented by dotted arrow.

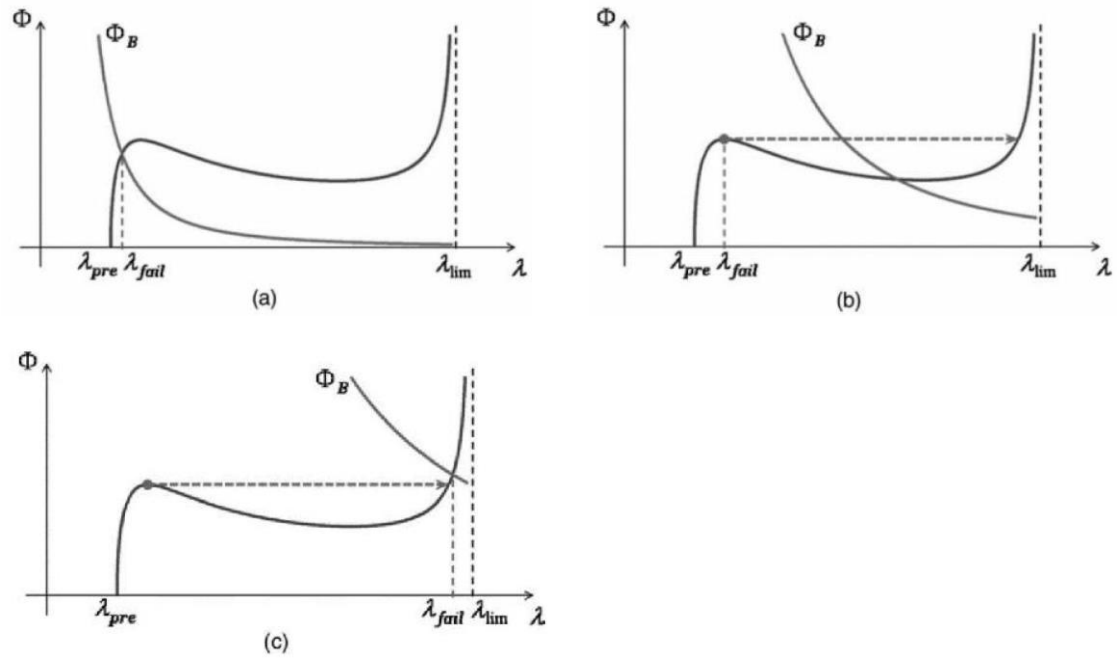

Figure 1.4 Electromechanical response and electric breakdown for three classes of DE membranes, (a) DE with low dielectric strength, (b) DE with moderate dielectric strength, (c) DE with high dielectric strength (Koh et al. 2011).

In order to improve the limit of the actuated deformation of DEs, researchers have proposed methods to tackle the EMI. By applying a pre-stretch, the actuation strain of a silicon dielectric elastomer plate increases from 30% ~ 40% to 117% (Kornbluh et al., 1999; Pelrine et al., 2000). When the pre-stretch is large enough, EMI can even be eliminated (Koh et al., 2011; Zhou, et al., 2013; Kollosche et al., 2012). Another common approach to avoid EMI is to apply proper boundary constraints to the DE membrane (Zhou, et al., 2013). Other alternatives to avoid EMI are also available in the literature, such as spraying charges on the compliant electrodes (Keplinger et al., 2010), reinforcing the DE with fibres, solvents and interpenetrating networks (Lu et al., 2012; Shankar et al., 2007; Huang et al., 2012b; Ha et al., 2006). However, in the applications of DEs, their actuated deformation, failure modes and dynamic performance are also significantly influenced by the intrinsic material viscoelasticity, which is still not well-understood. Therefore, to improve the performance of DE-based devices, further investigations accounting for their material viscoelasticity are needed.

1.3 Objectives

The ultimate goal of this work aims to provide guidance for the reliable design of DE oscillators and resonators. Detailed objectives are as follows: developing a theoretical model to account for their material viscoelasticity with consideration of multiple relaxation time; studying the dynamic performance of DE membrane resonators with different relaxation processes; investigating the frequency tuning and dynamic behaviours of DE membrane resonators and uncovering possible ways to improve their design.

1.4 Thesis structure

Following the introduction in Chapter 1, Chapter 2 presents a literature review and fundamentals. The studies on dielectric elastomers considering the material hyperelasticity and viscoelasticity are reviewed. Also, the modeling framework for finite-deformation

viscoelasticity of DEs is introduced in Chapter 2. In Chapter 3, the general viscoelastic model in Chapter 2 is specified to investigate the performance of DE membrane resonators. Last but not least, Chapter 4 summarizes this thesis and provides suggestions for the future work.

Chapter 2

2 Literature review

In recent years, much attention has been given to the potential use of DEs in soft robotics, medical and biomimetic equipment and energy harvesting systems. As a result, extensive work has been done to study the interplay of their electromechanical deformation, multiple failure modes and material viscoelasticity. This chapter reviews the existing studies on modelling the complex electromechanical coupling behaviours of DEs.

2.1 Hyperelasticity and fully coupled electromechanical field theory of DEs

Early studies on DEs assume that the stress induced by the electric field can be determined by the Maxwell pressure $P = \varepsilon\varepsilon_0 E^2$ (ε is the dielectric constant, ε_0 is the vacuum permittivity, E is the electric field induced by the applied voltage) (Pelrine, et al., 1998; Kornbluh, et al., 1999). Also, the relation between the strain and stress is assumed to be linear. However, the assumed linear constitutive relation between the stress and the strain is limited to account for small deformation, while is insufficient to describe the large deformation of dielectric elastomers. Later work assumed that the total stress in DEs is the summation of the stress associated with a strain energy density function of the material and the empirical Maxwell stress (Goulbourne et al., 2005 and 2007; Mockensturm and Goulbourne, 2006; Wissler, et al., 2005b; Ma and Cross, 2004; G. Yang, et al., 2005). For example, Goulbourne, Mockensturm, and Frecker (2005) proposed a non-linear model for axisymmetric DE membranes, in which the Mooney-Rivlin and the Ogden strain energy functions were adopted. Wissler and Mazza (2005b) studied the actuation of a pre-stretched circular DE actuator under uniaxial and biaxial tension, and compared the stresses obtained from the Yeoh, Ogden and Mooney-Rivlin models. Nevertheless, these uncoupled models are only capable of explaining some experimental results. Later, Dorfmann and Ogden (2005), McMeeking and Landis (2005) and Suo, Zhao, and Greene (2008) proposed the fully coupled field theory for the electromechanical response of DEs. In those models, the

strain energy density and the electric polarization are coupled in the Helmholtz free energy density. Moreover, most hyperelastic energy density functions can be adopted in the modelling framework based on the fully coupled field theory (Boyce and Arruda, 2000 and 1993; Boyce, 1996; Gent, 1996; Rivlin, 1948; Mooney, 1940; Yeoh, 1993; Ogden, 1972). The fully coupled field theory better explains the nonlinear electromechanical response of DEs and provides a solid foundation to further study the comprehensive performance of DEs.

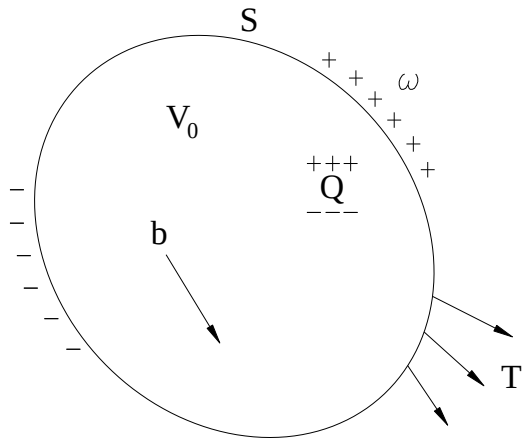

Figure 2.1 Illustration of a dielectric elastomer subject to body forces, surface tractions, and free charges.

The fully coupled field theory is outlined in the following section. Fig. 2.1 shows the current state of a dielectric elastomer subjected to the body force **b** (**X**, t), the surface traction **T** (**X**, t), and free charges. The volume of the dielectric body is V_0 and its surface is S. We denote $\boldsymbol{x}$ as the current position of an arbitrary material particle of the DE, and $\boldsymbol{X}$ as its reference or initial position. $Q(\boldsymbol{X}, t)$ is the density of the free volume charge and $\omega(\boldsymbol{X}, t)$ is the density of the free surface charge. The deformation gradient in the current state is described as,

$$\mathrm{F_{ik}} = \frac{\partial \mathrm{x_i}}{\partial \mathrm{X_k}} . \tag{2.1}$$

Introducing two arbitrary test functions $\xi_i(\mathbf{X})$ and $\eta(\mathbf{X})$,

$$\int_V \frac{\partial \xi_i}{\partial X_k} s_{ik} dV_0 = \int_S T_i \xi_i dS - \int_V \xi_i \frac{\partial s_{ik}}{\partial X_k} dV_0 , \tag{2.2}$$

$$\int_V \frac{\partial \eta}{\partial X_k} \tilde{D}_k dV_0 = -\int_S \omega \eta dS - \int_V \eta \frac{\partial \tilde{D}_k}{\partial X_k} dV_0 , \tag{2.3}$$

in which s_{ik} is the first Piola-Kirchhoff stress (nominal stress), and $\tilde{D}_k$ is the nominal electric displacement. The equation of motion gives

$$\frac{\partial s_{ik}}{\partial X_k} = -b_i + \rho \frac{d^2 x_i}{dt^2} . \tag{2.4}$$

Combining Eqs. (2.2) and (2.4) results in

$$\int_{V_0} \frac{\partial \xi_i}{\partial X_k} s_{ik} dV_0 = \int_S T_i \xi_i dS + \int_{V_0} \xi_i b_i dV_0 - \int_{V_0} \rho \frac{d^2 x_i}{dt^2} \xi_i dV_0 . \tag{2.5}$$

According to the Maxwell's law, the nominal electric field $\tilde{E}_k$ of the DE body must satisfy

$$\tilde{E}_k = -\frac{\partial \Phi}{\partial X_k} . \tag{2.6}$$

Also, the Gauss' law relates the nominal electric displacement $\tilde{D}_k$ and the free charge by

$$\frac{\partial \tilde{D}_k}{\partial X_k} = Q . \tag{2.7}$$

Combining Eq. (2.3) and (2.7) results in,

$$\int_{V_0} \frac{\partial \eta}{\partial X_k} \tilde{D}_k dV_0 = -\int_S \omega \eta dS - \int_{V_0} \eta Q dV_0 . \tag{2.8}$$

Therefore, the change of the total free energy G_f of the dielectric elastomer due to the small changes of the deformation and free charges can be expressed as

$$\delta G_f = \int_{V_0} \delta W dV_0 - \int_{V_0} b_i \delta x_i dV_0 - \int_S T_i \delta x_i dS - \int_{V_0} \delta Q \Phi dV_0 - \int_S \delta \omega \Phi dS + \int_{V_0} \rho \frac{d^2 x_i}{dt^2} \delta x_i dV_0 \,, \qquad (2.9)$$

where $\mathbf{W}(\mathbf{F}, \tilde{\boldsymbol{D}})$ is the Helmholtz free energy density. Considering δx_i and Φ in Eq. (2.9) as the test functions $\xi_i(\mathbf{X})$ and $\eta(\mathbf{X})$ in Eqs. (2.2) and (2.3), Eq. (2.9) is reduced to,

$$\delta G_f = \int_{V_0} \delta W dV_0 - \int_{V_0} \delta F_{ik} s_{ik} dV_0 - \int_{V_0} \tilde{E}_k \delta \tilde{D}_k dV_0 \,. \qquad (2.10)$$

Recalling $\delta W = \frac{\partial W}{\partial F_{ik}} \delta F_{ik} + \frac{\partial W}{\partial \tilde{D}_k} \delta \tilde{D}_k$, Eq. (2.10) is rewritten as

$$\delta G_f = \int_{V_0} (\frac{\partial W}{\partial F_{ik}} - s_{ik}) \delta F_{ik} dV_0 + \int_{V_0} (\frac{\partial W}{\partial \tilde{D}_k} - \tilde{E}_k) \delta \tilde{D}_k dV_0 \,. \qquad (2.11)$$

Minimizing the change of the free energy gives

$$s_{ik} = \frac{\partial W^{EQ}(\mathbf{F}, \tilde{\mathbf{D}})}{\partial F_{ik}} \,, \qquad (2.12)$$

$$\tilde{E}_k = \frac{\partial W^{EQ}(\mathbf{F}, \tilde{\mathbf{D}})}{\partial \tilde{D}_k} \,. \qquad (2.13)$$

The Helmholtz free energy density $\mathrm{W}(\mathrm{F}, \tilde{D})$ of the pure elastic dielectric material is equal to the sum of the strain energy density $W_s(\mathbf{F})$ and the polarization energy (Zhao *et al*., 2007), i.e.,

$$W(\mathbf{F}, \tilde{\mathbf{D}}) = W_s(\mathbf{F}) + \frac{F_{KM} F_{KL}}{2\varepsilon\varepsilon_0 \det(\mathbf{F})} \tilde{D}_M \tilde{D}_L \,. \qquad (2.14)$$

Then the true stress σ, the true electric displacement ***D***, and the true electric field ***E*** in the current state of the dielectric elastomer can be determined by the relations between true and nominal quantities i.e.,

$$\sigma_{ij} = \frac{F_{jk}}{\det(\mathbf{F})} s_{ik}, \tag{2.15}$$

$$D_i = \frac{F_{ik}}{\det(\mathbf{F})} \tilde{D}_k, \tag{2.16}$$

$$E_i = H_{ik} E_k, \tag{2.17}$$

in which $F_{ik} H_{ik} = 1$.

2.2 Viscoelastic DEs with single relaxation process

Other than hyperelasticity, theoretical and experimental studies have shown that DEs also possess strong viscoelasticity (Plante and Dubowsky, 2007; Zhang, et al., 2004, Bai et al., 2014, Kollosche, et al., 2015). Early modelling works on the viscoelasticity of DEs only account for their small deformation, e.g. the quasi-linear model for the viscoelastic DE membranes proposed by Wissler and Mazza (2005b). Later, researchers started to tackle the finite-deformation viscoelasticity of DEs. Based on the finite-deformation viscoelasticity theory of Christensen (1980), Yang et al. (2005) studied the nonlinear viscoelastic deformation of DE membranes. Recently, based on the fully coupled electromechanical field theory by Suo, et al. (2008) and the finite-deformation viscoelasticity theory by Reese and Govindjee (1998), Hong (2011) developed a constitutive model for viscoelastic DEs, which is capable of adopting most of the hyperelastic energy functions and thermodynamic evolution laws.

Fig. 2.2 depicts the rheology model of viscoelastic DEs (Hong, 2011). In the rheology model, the purely elastic ground network is represented by spring 1 and the viscous subnetwork is represented by spring 2 and the dashpot. Therefore, the total Helmholtz free energy density of the elastomer consists of two parts: the equilibrium Helmholtz free

energy density W^{EQ} (from spring 1 and the electric polarization) and the non-equilibrium Helmholtz free energy density W^{NEQ} (from spring 2). The dashpot relaxes with time, leading to the energy dissipation and stress relaxation of the elastomer.

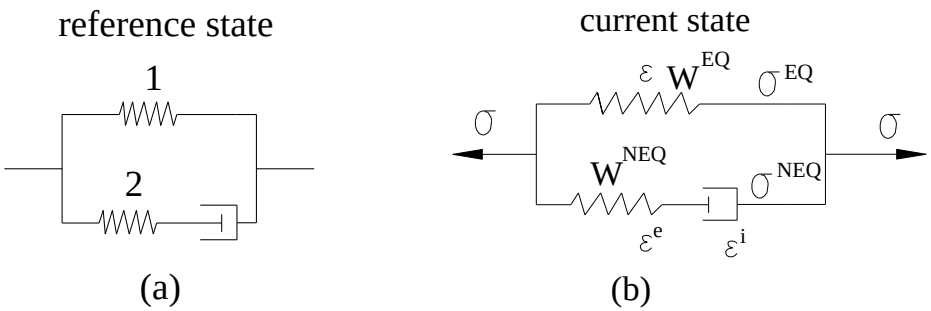

Figure 2.2 Rheology model for the viscoelastic material of polymer networks with single relaxation process.

Moreover, according to the work of Lee (1969) and the finite-deformation viscoelasticity theory of Reese and Govindjee (1998), the total deformation gradient of the DE can be expressed as the multiplication of the elastic deformation gradient and the inelastic deformation gradient, i.e.,

$$F_{ik} = F^{e}_{im} F^{i}_{mk}\,, \tag{2.18}$$

where the superscripts ‘e’ and ‘i’ represent elastic and inelastic, respectively. Also, the total Helmholtz free energy density can be expressed as

$$W\left(\mathbf{F},\mathbf{F}^{i},\tilde{\mathbf{D}}\right) = W^{EQ}\left(\mathbf{F},\tilde{\mathbf{D}}\right) + W^{NEQ}\left(\mathbf{F}\mathbf{H}^{i}\right), \tag{2.19}$$

where $\mathbf{H} = (\mathbf{F})^{-1}$, $\mathbf{H}^{i} = (\mathbf{F}^{i})^{-1}$ and $\mathbf{H}^{e} = (\mathbf{F}^{e})^{-1}$. Following Reese and Govindjee (1998), the inelastic deformation gradient must satisfy the thermodynamic evolution equation,

$$-\frac{1}{2}\mathbf{F}\frac{d\left[\left(\mathbf{C}^{i}\right)^{-1}\right]}{dt}\mathbf{F}^{T}\left(\mathbf{b}^{e}\right)^{-1} = \boldsymbol{\gamma}^{-1} : \boldsymbol{\tau}_{NEQ}\,, \tag{2.20}$$

where $\mathbf{C}^i = \left(\mathbf{F}^i\right)^T \mathbf{F}^i$, $\left(\mathbf{b}^e\right)^{-1} = \left(\mathbf{H}^e\right)^T \mathbf{H}^e$, $\tau_{NEQ} = 2\mathbf{F}^e \frac{\partial W^{NEQ}}{\partial \mathbf{C}^e} \left(\mathbf{F}^e\right)^T$ and $\boldsymbol{\gamma}^{-1}$ is an isotropic rank four tensor. Here $\boldsymbol{\gamma}^{-1}$ takes the form

$$\boldsymbol{\gamma}^{-1} = \frac{1}{2\eta_D}\left(\mathbf{I}^4 - \frac{1}{3}\mathbf{I}\otimes\mathbf{I}\right) + \frac{1}{9\eta_V}\mathbf{I}\otimes\mathbf{I}, \tag{2.21}$$

$\mathbf{I}^4 = \frac{1}{2}\left(\delta_{ik}\delta_{jl} + \delta_{il}\delta_{jk}\right)$ is the fourth order symmetric identity tensor, I is the second order identity tensor, η_D and η_V represent the deviatoric and volumetric viscosities, respectively. Based on the finite-deformation viscoelasticity modelling framework above, Park et al. (2012 and 2013) developed a finite element model to study the inhomogenious deformation of DEs. With the FEM model of Park et al. (2012), Wang et al. (2013) investigated the creep behaviour and electromechanical instability of DEs.

2.3 Viscoelastic DEs with multiple relaxation processes

For the theoretical framework above, the material is assumed to have one purely elastic ground network and one viscous subnetwork. However, elastomers are known to have multiple relaxation processes, which could not be captured with a single viscous subnetwork. Furthermore, experiments have suggested that elastomeric materials have a wide range of relaxation times and it is necessary to consider multiple relaxation processes of dielectric elastomers to predict their dynamic behaviours(Liu et al., 2015; Guo et al., 2015; Michel et al., 2010; Wissler and Mazza, 2007; Zhang, 2018; Zhang, et al., 2014, 2017b and 2017c). For example, Zhang (2018) did frequency testings for VHB 4910 films and found that the model considering three relaxation processes improve the accuracy of prediction for the frequency response by 80% compared to the model with single relaxation process. Michel (2010) and Wissler (2007) proposed that the relaxation time of VHB polymer elastomers can range from a few seconds to hundreds of seconds or even longer. Therefore, a model with the consideration of multiple viscous subnetworks is needed to better capture the viscoelastic behaviours of DEs. A modified rheological model with multiple viscous subnetworks of DEs is shown in Fig. 2.3. The material viscosity for each

viscous subnetwork could be different, which result in multiple relaxation times of DEs. As shown in Fig. 2.3, the total Helmholtz free energy density of the DE equals the sum of the Helmholtz free energy density of each network, which results in

$$W\left(\mathbf{F},\mathbf{F}^{i},\tilde{\mathbf{D}}\right)=W^{EQ}\left(\mathbf{F},\tilde{\mathbf{D}}\right)+\sum_{m=1}^{n}W_{m}^{NEQ}\left(\mathbf{F}\mathbf{H}^{i}{}_{m}\right). \tag{2.22}$$

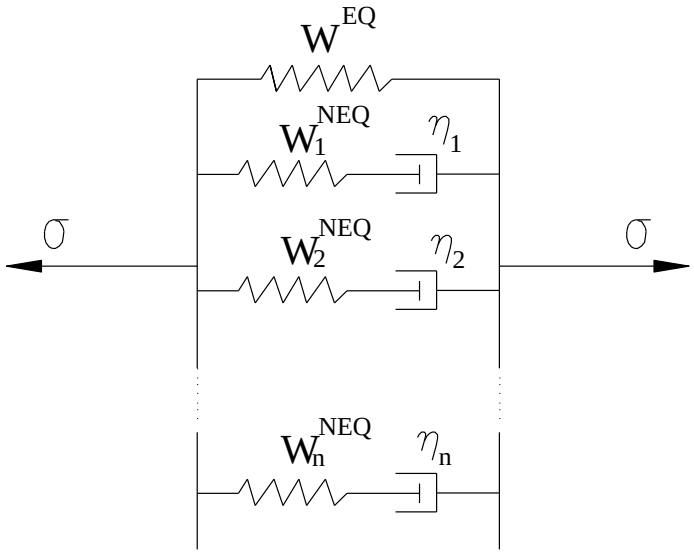

Figure 2.3 Rheology model for the viscoelastic DE of polymer networks with multiple viscous subnetworks.

From the literature review above, it can be seen that much effort has been devoted to studying the hyperelasticity and viscoelasticity of DEs. However, their effects on DE-based devices are still not well-understood, especially on the dynamic performance of DE oscillators or resonators. To tackle this unsettled issue, modelling and simulation of a DE membrane resonator considering material viscoelasticity with multiple relaxation processes will be presented in the following chapter.

Chapter 3

3 Effect of the material viscoelasticity on the frequency tuning of the dielectric elastomer membrane resonators

3.1 Introduction

As soft electroactive polymers, dielectric elastomers (DEs) response to electrical stimuli. Due to this property of DEs, they have been developed as resonators and oscillators (Suo, 2010; Hong and Suo, 2007; Romasanta et al., 2015; Ahmadi et al., 2013; Anderson et al., 2010; Chiba et al., 2011; Heydt et al., 2006; Huang et al., 2013; Karsten et al., 2013; Bastawros and Hong, 2012). For DE resonators and oscillators, their resonant frequency and vibrating modes can be actively tuned by the applied voltage, which could be a desirable solution to the compensation for fabrication and environmental imperfection (Dubois et al., 2008; Son and Goulbourne 2010; Bonwit, 2006; O'Brien, 2012; Zhang, 2005).

In the literature, many studies have considered the material hyper-elasticity to investigate the dynamic and tuneable behaviour of dielectric elastomers. For example, Mockensturn and Goulbourne (2006) studied the dynamic response of an axisymmetric spherical membrane resonator using the Mooney model. Fox and Goulbourne (2008 and 2009) carried out numerical simulation and experimental study on the dynamic response of a membrane resonator with both the Mooney–Rivlin and the Ogden models. Zhu et al. (2010a and 2010b) studied the nonlinear oscillation and natural frequency tuning of a spherical DE membrane. Yong et al. (2011) explored the nonlinear oscillation of spherical DE membranes with a Neo-Hookean model. The resonant frequency tuning of a DE micro-beam with small and large vibration amplitude was studied by Feng et al. (2011 and 2013). Li, Qu, and Yang (2012) demonstrated the natural frequency tuning and oscillation of a DE membrane resonator with the Gent model.

However, less effort has been devoted to exploring the viscoelastic effect of DEs, which has been proven to strongly affect the dynamic and resonant performance of DE oscillators and resonators (Zhou, et al., 2014 and 2016b; Zhang, et al., 2017a and 2017b). Zhou, et al. (2014 and 2016b) studied the viscoelastic effect on DE resonators and oscillators considering single relaxation process with a standard viscoelasticity model. Zhang, et al. (2017a) investigated the influence of viscous damping with the Kelvin-Voigt model on the vibration of DEs. Zhang, et al. (2017b) applied Kelvin-Voigt-Maxwell model to investigate the single viscoelastic creep and relaxation process of a DE membrane. As well-established, DEs exhibit strong viscoelastic property (cf., e.g., Wissler and Mazza, 2005a; Kornbluh et al., 2000; Zhang, et al., 2015; Wang, et al., 2013; Bai, et al., 2014, Vogel et al.,2014, among many others), which originates from the highly mobile polymer chains that form their polymer networks (Linder, et al., 2011; Li, et al., 2016; Wang et al., 2016; Cohen et al., 2016). For example, Zhang, et al. (2015) showed that the resonant behavior and vibration of DE membranes under electric field and different mechanical loading states are highly time-dependent due to the material viscoelasticity. Wang, et al. (2013) explored the inhomogenous viscoelastic deformation of DE circular membranes. The constitutive model proposed by Linder, et al. (2011) for viscoelastic rubber-like materials was based on the diffusion processes of the flexible polymer chains. Based on the model of Linder, et al. (2011), Wang et al. (2016) studied the time-dependent effect of VHB4910 on large deformation and electromechanical instabilities by considering the material viscoelasticity and polymer chain microstructres. The polymer networks in DEs are commonly idealized as one purely elastic ground network and a few viscous subnetworks (Zhou, et al., 2018; Gerhard, 2000; Zhang, et al., 2017c; Linder, et al., 2011). Due to the multiple viscous subnetworks structure, DEs possess multiple relaxation times during the deformation (Guo, et al., 2015; Xiao, 2016; Hossain, et al., 2012 and 2015; Liu, et al., 2015), and the relaxation time for the polymer subnetworks can range from a few seconds to hundreds of seconds or even longer (Zhao et al., 2011; Michel et al., 2010; Wissler et al., 2007). Hossain et al. (2012 and 2015) demonstrated the time-dependent characterization of VHB 4910 by stress-relaxation experiments and rate-dependent responses. Guo et al. (2015) and Xiao (2016) developed theoretical models with multiple relaxation processes of VHB 4905 membranes to study the temperature effect on their deformation. Nevertheless, most of the existing

modelling works on viscoelastic dielectric elastomers only consider a single viscous subnetwork (Hong, 2011; Zhou, et al., 2014 and 2016b; Zhang, et al., 2017b), which may lead to significant error when evaluating the performance of DE oscillators and resonators. Khan et al. (2013) stated that models with a single relaxation process is physically insufficient to capture the electromechanical responses and predict the critical condition of EMI for DEs. Zhang (2018) presented that a model with three relaxation processes could improve the accuracy by 80% in frequency responses prediction for DEs. Therefore, in order to predict the dynamic and resonant performance of DE resonators and oscillators, it is essential to develop a modelling framework that can account for their multiple relaxation processes.

Based on the theoretical framework of Hong (2011) and employing Gent hyperelastic model (Gent, 1996), a modelling framework is developed in the current work to investigate the multi-relaxation effect on a viscoelastic DE membrane resonator, especially on its resonant frequency tuning process. In addition, the interplay among the pre-stretch effect, the material viscoelasticity and the failure modes (electrical breakdown and loss-of-tension) of DEs are also studied in the modelling process. It should be mentioned that the electromechanical instability (EMI) is not considered here since it is avoided due to the boundary constraints of the resonator configuration (Zhou, et al., 2013; Koh, et al., 2011; Kollosche, et al., 2012).

3.2 Formulation of the DE Membrane Resonator

The configuration of a DE membrane resonator is illustrated in Fig. 3.1(Biggs and Hitchcock, 2010; Li, et al., 2012). An undeformed DE membrane (Fig. 3.1(a)) with dimensions L_1, L_2, and L_3 ($L_3 \ll L_1, L_2$) is pre-stretched to l_1 and l_2 in 1 and 2 directions, respectively. The corresponding pre-stretch ratios are defined as $\lambda_{1p} = l_1/L_1$ and $\lambda_{2p} = l_2/L_2$ (Fig. 3.1(b)). The pre-stretched membrane is retained with a rigid frame and clamped with two rigid bars of mass *m* to divide the membrane into two parts A and B (Fig. 3.1(c)). Membrane A is coated with compliant electrodes on its both surfaces (shaded area). The lengths of membrane A and B in 1-direction are denoted as L_{1A} and L_{1B} respectively,

with the length ratio denoted as $k = L_{1A}/L_{1B}$ (Fig. 3.1(c)). When a voltage V is applied to the electrodes of membrane A, both membrane A and B deform in 1-direction to the current state with lengths l_{1A} and l_{1B}, respectively (Fig. 3.1(d)). The corresponding stretch ratios are calculated as $\lambda_{1A} = l_{1A}/L_{1A}$ and $\lambda_{1B} = l_{1B}/L_{1B}$. At the current state, membrane A is subjected to the tensile forces P_{1A} and P_{2A} in 1 and 2-direction respectively, and the electric loading V; the membrane B is subjected to tensile forces P_{1B} and P_{2B}. The stretch ratios of membrane A and B satisfy $\lambda_{1B} = \lambda_{1p} + k\left(\lambda_{1p} - \lambda_{1A}\right)$, and $\lambda_{2A} = \lambda_{2B} = \lambda_{2p}$ since the pre-stretch in 2-direction is assumed to be fixed by the rigid frame.

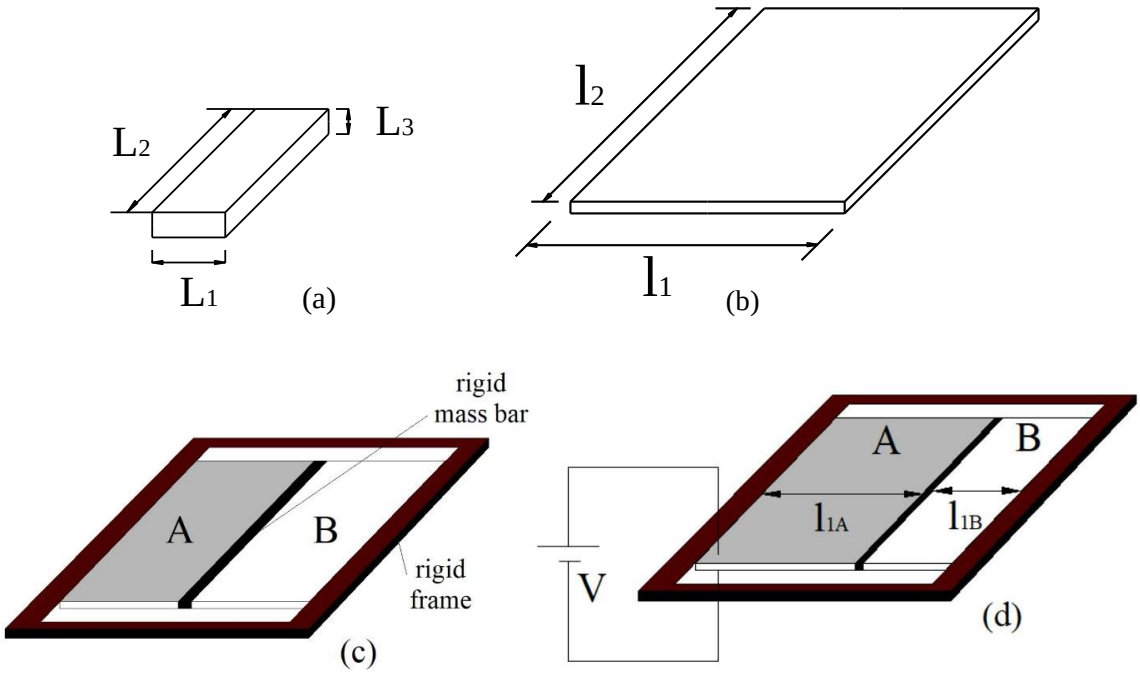

Figure 3.1 Schematic illustration of the DE membrane resonator: (a) unstrained reference state; (b) pre-stretch state; (c) the pre-stretched membrane is confined with a rigid frame in 2-direction and divided into A and B parts by the bonded two rigid mass bars; (d) current actuation state with electric loading V applied to membrane part A.

Under actuation, the total deformation gradients of membrane A and B at the current state with relative to the undeformed state are written as

$$\mathbf{F}^A = \begin{pmatrix} \lambda_{1A} & 0 & 0 \\ 0 & \lambda_{2A} & 0 \\ 0 & 0 & \lambda_{3A} \end{pmatrix}, \tag{3.1a}$$

and

$$\mathbf{F}^B = \begin{pmatrix} \lambda_{1B} & 0 & 0 \\ 0 & \lambda_{2B} & 0 \\ 0 & 0 & \lambda_{3B} \end{pmatrix}. \tag{3.1b}$$

According to the study of Lee (1969), the total deformation gradient can be multiplicatively split into an elastic part and a viscous part (Hong, 2011; Reese and Govindjee, 1998). Therefore, for each viscous polymer subnetwork (see Fig. 2.3), $\mathbf{F}_A = \mathbf{F}_{Am}^e \mathbf{F}_{Am}^i$ and $\mathbf{F}_B = \mathbf{F}_{Bm}^e \mathbf{F}_{Bm}^i$, where m=1, 2, …, n, and the superscripts 'e' and 'i' represent elastic and inelastic, respectively. Expressing the deformation gradients in terms of the stretch ratios gives that

$$\mathbf{F}_{Am}^e = \begin{pmatrix} \lambda_{1Am}^e & 0 & 0 \\ 0 & \lambda_{2Am}^e & 0 \\ 0 & 0 & \lambda_{3Am}^e \end{pmatrix}, \tag{3.1c}$$

$$\mathbf{F}_{Am}^i = \begin{pmatrix} \lambda_{1Am}^i & 0 & 0 \\ 0 & \lambda_{2Am}^i & 0 \\ 0 & 0 & \lambda_{3Am}^i \end{pmatrix}, \tag{3.1d}$$

and

$$\mathbf{F}_{Bm}^e = \begin{pmatrix} \lambda_{1Bm}^e & 0 & 0 \\ 0 & \lambda_{2Bm}^e & 0 \\ 0 & 0 & \lambda_{3Bm}^e \end{pmatrix}, \tag{3.1e}$$

$$\mathbf{F}_{Bm}^{i}=\begin{pmatrix}\lambda_{1Bm}^{i} & 0 & 0\\ 0 & \lambda_{2Bm}^{i} & 0\\ 0 & 0 & \lambda_{3Bm}^{i}\end{pmatrix}. \tag{3.1f}$$

DEs are commonly assumed to be incompressible for both elastic and inelastic deformation in many existing studies (Wissler and Mazza, 2005; Plante and Dubowsky, 2006; Zhao and Suo, 2007; Zhao, et al., 2007; Zhu, et al., 2010; Zhao and Suo, 2010; Hong, 2011; Koh, et al., 2011; Lu, et al., 2012; Huang and Suo, 2012; Zhou, et al., 2013). Adopting the same assumption, the deformation gradients above depend solely on the stretch ratios in 1 and 2-direction, i.e., $\lambda_{3A}=1/\lambda_{1A}\lambda_{2A}$, $\lambda_{3Am}^{e}=1/\lambda_{1Am}^{e}\lambda_{2Am}^{e}$, $\lambda_{3Am}^{i}=1/\lambda_{1Am}^{i}\lambda_{2Am}^{i}$, $\lambda_{3B}=1/\lambda_{1B}\lambda_{2B}$, $\lambda_{3Bm}^{e}=1/\lambda_{1Bm}^{e}\lambda_{2Bm}^{e}$, and $\lambda_{3Bm}^{i}=1/\lambda_{1Bm}^{i}\lambda_{2Bm}^{i}$.

The finite-deformation viscoelasticity theory by Reese and Govindjee (1998) suggests that the Helmholtz free energy density W of the DE membrane at the current actuation state can be split into the non-equilibrium Helmholtz free energy density W^{NEQ} and the equilibrium Helmholtz free energy density W^{EQ}. W^{NEQ} is determined by the elastic deformation of all the polymer subnetworks and W^{EQ} depends on the total deformation of the purely elastic ground network of and the electric displacement D. For membrane A, The Helmholtz free energy density under the electric loading is expressed as

$$W_A=W_A^{EQ}(\lambda_{1A},\lambda_{2A},D)+\sum_{m=1}^{n}W_A^{NEQ}{}_m(\lambda_{1Am}^{e},\lambda_{2Am}^{e}), \tag{3.2}$$

where $W^{NEQ}=\sum_{m=1}^{n}W_A^{NEQ}{}_m(\lambda_{1Am}^{e},\lambda_{2Am}^{e})$. The electric field is assumed to be always in equilibrium since it is commonly agreed that it reaches equilibrium much faster than mechanical deformations (Zhou, 2015; Zhou et al., 2014, 2016b). Therefore, the equilibrium Helmholtz free energy density W_A^{EQ} $(\lambda_{1A}, \lambda_{2A}, D)$ consists of the strain energy density W_S $(\lambda_{1A}, \lambda_{2A})$ from the total deformation of the membrane and the energy density $D^2/(2\varepsilon\varepsilon_0)$ from electric polarization (Huang and Suo, 2012; Hong, 2011), i.e.,

$$W_A^{EQ}(\lambda_{1A},\lambda_{2A},D)=W_s\left(\lambda_{1A},\lambda_{2A}\right)+\frac{D^2}{2\varepsilon\varepsilon_0}, \tag{3.3}$$

where ε is the permittivity of the vacuum, ε_0 is the relative dielectric material constant. The electric field D is assumed to be uniformly distributed (Lu, et al., 2012; Koh, et al., 2011). Applying the relation between the electric field E and the voltage V i.e., $E=\frac{V_A}{L_3}\lambda_{1A}\lambda_{2A}$, and the material law between the electric field E and electric displacement D, i.e., $D=\varepsilon\varepsilon_0 E$ (Zhao, et al., 2007; Huang and Suo, 2012), Eq. (3.2) can be further expressed as

$$W_A=W_s\left(\lambda_{1A},\lambda_{2A}\right)+\sum_{m=1}^{n}W_A^{NEQ}{}_m(\lambda_{1A}/\lambda_{1Am}^{i},\lambda_{2A}/\lambda_{2Am}^{i})+\frac{\varepsilon\varepsilon_0}{2}\left(\frac{V_A}{L_3}\right)^2\lambda_{1A}^2\lambda_{2A}^2. \tag{3.4}$$

During the actuation state for membrane A, the change of the Helmholtz free energy density W_A resulting from any small change of the stretch ratios (denoted as $\delta\lambda_{1A}$ and $\delta\lambda_{2A}$ in 1 and 2-direction, respectively) is equal to the work done by the tensile forces P_{1A}, P_{2A}, the inertial force, and the voltage V. It is thus expressed as

$$\begin{aligned}&L_{1A}L_2L_3\left(\frac{\partial W_A}{\partial\lambda_{1A}}\delta\lambda_{1A}+\frac{\partial W_A}{\partial\lambda_{2A}}\delta\lambda_{2A}\right)\\&=P_{1A}L_{1A}\delta\lambda_{1A}+P_{2A}L_2\delta\lambda_{2A}-L_2L_3\frac{L_{1A}^3}{3}\rho\frac{d^2\lambda_{1A}}{dt^2}\delta\lambda_{1A}-L_{1A}L_2\frac{L_3^3}{3}\rho\frac{d^2\left(\lambda_{1A}^{-1}\lambda_{2A}^{-1}\right)}{dt^2}\delta\left(\lambda_{1A}^{-1}\lambda_{2A}^{-1}\right)\cdot\\&+L_{1A}L_2L_3\left[2\varepsilon\varepsilon_0\left(\frac{V_A}{L_3}\right)^2\lambda_{1A}\lambda_{2A}^2\delta\lambda_{1A}+2\varepsilon\varepsilon_0\left(\frac{V_A}{L_3}\right)^2\lambda_{1A}^2\lambda_{2A}\delta\lambda_{2A}\right]\end{aligned} \tag{3.5}$$

where ρ is the material density. When the film is very thin ($L_3\ll L_1$), the last term in Eq. (3.5) can be neglected (Li et al., 2012). Combining Eq. (3.4), Eq. (3.5) gives

$$\begin{aligned}&\left\{L_AL_2L_3\left[\frac{\partial W_s}{\partial\lambda_{1A}}+\sum_{m=1}^{n}\frac{\partial W_A^{NEQ}{}_m}{\partial\lambda_{1Am}^{e}}\lambda_{1A}^{i-1}{}_m-\varepsilon\varepsilon_0\left(\frac{V_A}{L_3}\right)^2\lambda_{1A}\lambda_{2A}^2\right]-P_{1A}L_{1A}+L_2L_3\frac{L_1^3}{3}\rho\frac{d^2\lambda_{1A}}{dt^2}\right\}\delta\lambda_{1A}\\&+\left\{L_AL_2L_3\left[\frac{\partial W_s}{\partial\lambda_{2A}}+\sum_{m=1}^{n}\frac{\partial W_A^{NEQ}{}_m}{\partial\lambda_{2Am}^{e}}\lambda_{2A}^{i-1}{}_m-\varepsilon\varepsilon_0\left(\frac{V_A}{L_3}\right)^2\lambda_{2A}\lambda_{1A}^2\right]-P_{2A}L_2\right\}\delta\lambda_{2A}=0.\end{aligned} \tag{3.6}$$

The change of the stretch ratios ($\delta\lambda_{1A}$ and $\delta\lambda_{2A}$) are small and arbitrary, which yields

$$L_A L_2 L_3 \left[\frac{\partial W_s}{\partial \lambda_{1A}} + \sum_{m=1}^{n} \frac{\partial W_A^{NEQ}{}_m}{\partial \lambda_{1Am}^e} \lambda_{1A}^{i-1}{}_m - \varepsilon\varepsilon_0 \left(\frac{V_A}{L_3} \right)^2 \lambda_{1A} \lambda_{2A}^2 \right] - P_{1A} L_{1A} + L_2 L_3 \frac{L_1^3}{3} \rho \frac{d^2 \lambda_{1A}}{dt^2} = 0, \tag{3.7}$$

$$L_A L_2 L_3 \left[\frac{\partial W_s}{\partial \lambda_{2A}} + \sum_{m=1}^{n} \frac{\partial W_A^{NEQ}{}_m}{\partial \lambda_{2Am}^e} \lambda_{2A}^{i-1}{}_m - \varepsilon\varepsilon_0 \left(\frac{V_A}{L_3} \right)^2 \lambda_{2A} \lambda_{1A}^2 \right] - P_{2A} L_2 = 0. \tag{3.8}$$

Adopting the Gent model (Gent, 1996) as the strain energy density function for membrane A, i.e.,

$$W_s = -\frac{G^{EQ} J_{\lim}}{2} \ln \left(1 - \frac{\lambda_{1A}^2 + \lambda_{2p}^2 + \lambda_{1A}^{-2} \lambda_{2A}^{-2} - 3}{J_{\lim}} \right), \tag{3.9}$$

where G^{EQ} is the equilibrium shear modulus and J_{lim} is a dimensionless stretch limit parameter of the DE material. Following the work of Hong (2011), the non-equilibrium Helmholtz free energy density for each polymer subnetwork can be expressed as

$$W_A^{NEQ}{}_m = -\frac{G^{NEQ}{}_m J_{\lim}}{2} \ln \left(1 - \frac{\left(\lambda_{1Am}^e \right)^2 + \left(\lambda_{2Am}^e \right)^2 + \left(\lambda_{1Am}^e \lambda_{2Am}^e \right)^{-2} - 3}{J_{\lim}} \right), \tag{3.10}$$

G_m^{NEQ} is the non-equilibrium shear modulus for each polymer subnetwork. Combining Eqs. (3.7) ~ (3.10), we can obtain the stresses of membrane A as

$$\begin{aligned} \frac{P_{1A}}{G L_2 L_3} &= \frac{\chi J_{\lim} \left(\lambda_{1A} - \lambda_{1A}^{-3} \lambda_{2A}^{-2} \right)}{J_{\lim} - \lambda_{1A}^2 - \lambda_{2A}^2 - \lambda_{1A}^{-2} \lambda_{2A}^{-2} + 3} \\ &+ \sum_{m=1}^{n} \frac{G^{NEQ}{}_m}{G} \frac{J_{\lim} \left[\lambda_{1A} \left(\lambda_{1Am}^i \right)^{-2} - \lambda_{1A}^{-3} \lambda_{2A}^{-2} \left(\lambda_{1Am}^i \lambda_{2Am}^i \right)^2 \right]}{J_{\lim} - \left(\frac{\lambda_{1A}}{\lambda_{1Am}^i} \right)^2 - \left(\frac{\lambda_{2A}}{\lambda_{2Am}^i} \right)^2 - \left(\frac{\lambda_{1A} \lambda_{2A}}{\lambda_{1Am}^i \lambda_{2Am}^i} \right)^{-2} + 3} \\ &+ \frac{L_{1A}^2}{3G} \rho \frac{d^2 \lambda_{1A}}{dt^2} - \frac{\varepsilon\varepsilon_0}{G} \left(\frac{V_A}{L_3} \right)^2 \lambda_{1A} \lambda_{2A}^2, \end{aligned} \tag{3.11}$$

$$\frac{P_{2A}}{GL_AL_3}=\frac{\chi J_{\lim}\left(\lambda_{2A}-\lambda_{2A}^{-3}\lambda_{1A}^{-2}\right)}{J_{\lim}-\lambda_{1A}^2-\lambda_{2A}^2-\lambda_{1A}^{-2}\lambda_{2A}^{-2}+3}+$$
$$\sum_{m=1}^{n}\frac{G^{NEQ}{}_m}{G}\frac{J_{\lim}\left[\lambda_{2A}\left(\lambda_{2Am}^i\right)^{-2}-\lambda_{2A}^{-3}\lambda_{1A}^{-2}\left(\lambda_{1Am}^i\lambda_{2Am}^i\right)^2\right]}{J_{\lim}-\left(\frac{\lambda_{1A}}{\lambda_{1Am}^i}\right)^2-\left(\frac{\lambda_{2A}}{\lambda_{2Am}^i}\right)^2-\left(\frac{\lambda_{1A}\lambda_{2A}}{\lambda_{1Am}^i\lambda_{2Am}^i}\right)^{-2}+3} \tag{3.12}$$
$$-\frac{\varepsilon\varepsilon_0}{G}\left(\frac{V_A}{L_3}\right)^2\lambda_{2A}\lambda_{1A}^2,$$

where material parameters $G=G^{EQ}+G^{NEQ}, G^{NEQ}=\sum_{m=1}^{n}G^{NEQ}{}_m$ and $\chi=G^{EQ}/G$. χ is the fraction of the purely elastic ground polymer networks (Bergstrom and Boyce, 1998). For pure elastic material, χ =1. Similarly, the stresses of membrane B can be obtained as

$$\frac{P_{1B}}{GL_2L_3}=\frac{\chi J_{\lim}\left(\lambda_{1B}-\lambda_{1B}^{-3}\lambda_{2B}^{-2}\right)}{J_{\lim}-\lambda_{1B}^2-\lambda_{2B}^2-\lambda_{1B}^{-2}\lambda_{2B}^{-2}+3}$$
$$+\sum_{m=1}^{n}\frac{G^{NEQ}{}_m}{G}\frac{J_{\lim}\left[\lambda_{1B}\left(\lambda_{1Bm}^i\right)^{-2}-\lambda_{1B}^{-3}\lambda_{2B}^{-2}\left(\lambda_{1Bm}^i\lambda_{2Bm}^i\right)^2\right]}{J_{\lim}-\left(\frac{\lambda_{1B}}{\lambda_{1Bm}^i}\right)^2-\left(\frac{\lambda_{2B}}{\lambda_{2Bm}^i}\right)^2-\left(\frac{\lambda_{1B}\lambda_{2B}}{\lambda_{1Bm}^i\lambda_{2Bm}^i}\right)^{-2}+3} \tag{3.13}$$
$$+\frac{L_{1B}^2}{3G}\rho\frac{d^2\lambda_{1B}}{dt^2},$$

$$\frac{P_{2B}}{GL_BL_3}=\frac{\chi J_{\lim}\left(\lambda_{2B}-\lambda_{2B}^{-3}\lambda_{1B}^{-2}\right)}{J_{\lim}-\lambda_{1B}^2-\lambda_{2B}^2-\lambda_{1B}^{-2}\lambda_{2B}^{-2}+3}+$$
$$\sum_{m=1}^{n}\frac{G^{NEQ}{}_m}{G}\frac{J_{\lim}\left[\lambda_{2B}\left(\lambda_{2Bm}^i\right)^{-2}-\lambda_{2B}^{-3}\lambda_{1B}^{-2}\left(\lambda_{1Bm}^i\lambda_{2Bm}^i\right)^2\right]}{J_{\lim}-\left(\frac{\lambda_{1B}}{\lambda_{1Bm}^i}\right)^2-\left(\frac{\lambda_{2B}}{\lambda_{2Bm}^i}\right)^2-\left(\frac{\lambda_{1B}\lambda_{2B}}{\lambda_{1Bm}^i\lambda_{2Bm}^i}\right)^{-2}+3}. \tag{3.14}$$

The oscillation of the resonator is represented by the vibration of the rigid bars in 1-direction, and the rigid bars are subjected to forces P_{1A}, P_{1B} and the inertial force. The motion equation of the rigid bars is expressed as

$$\frac{P_{1A}}{GL_2L_3}-\frac{P_{1B}}{GL_2L_3}+\frac{mL_{1A}}{GL_2L_3}\frac{d^2\lambda_{1A}}{dt^2}=0\,. \tag{3.15}$$

However, when the membranes are in a static state, the inertia terms in Eq. (3.11) and Eq. (3.13) become 0 and forces P_{1A} and P_{1B} in Eq. (3.15) are in balance, i.e., $P_{1A}/GL_2L_3=P_{1B}/GL_2L_3$. Combining Eq. (3.11), Eq. (3.13) and Eq. (3.15), we obtain

$$\begin{aligned}
&\frac{\chi J_{\lim}\left(\lambda_{1A}-\lambda_{1A}^{-3}\lambda_{2A}^{-2}\right)}{J_{\lim}-\lambda_{1A}^2-\lambda_{2A}^2-\lambda_{1A}^{-2}\lambda_{2A}^{-2}+3}\\
&+\sum_{m=1}^{n}\frac{G^{NEQ}{}_m}{G}\frac{J_{\lim}\left[\lambda_{1A}\left(\lambda_{1Am}^i\right)^{-2}-\lambda_{1A}^{-3}\lambda_{2A}^{-2}\left(\lambda_{1Am}^i\lambda_{2Am}^i\right)^2\right]}{J_{\lim}-\left(\frac{\lambda_{1A}}{\lambda_{1Am}^i}\right)^2-\left(\frac{\lambda_{2A}}{\lambda_{2Am}^i}\right)^2-\left(\frac{\lambda_{1A}\lambda_{2A}}{\lambda_{1Am}^i\lambda_{2Am}^i}\right)^{-2}+3}-\frac{\varepsilon\varepsilon_0}{G}\left(\frac{V_A}{L_3}\right)^2\lambda_{1A}\lambda_{2A}^2\\
&=\frac{\chi J_{\lim}\left(\lambda_{1B}-\lambda_{1B}^{-3}\lambda_{2B}^{-2}\right)}{J_{\lim}-\lambda_{1B}^2-\lambda_{2B}^2-\lambda_{1B}^{-2}\lambda_{2B}^{-2}+3}\\
&+\sum_{m=1}^{n}\frac{G^{NEQ}{}_m}{G}\frac{J_{\lim}\left[\lambda_{1B}\left(\lambda_{1Bm}^i\right)^{-2}-\lambda_{1B}^{-3}\lambda_{2B}^{-2}\left(\lambda_{1Bm}^i\lambda_{2Bm}^i\right)^2\right]}{J_{\lim}-\left(\frac{\lambda_{1B}}{\lambda_{1Bm}^i}\right)^2-\left(\frac{\lambda_{2B}}{\lambda_{2Bm}^i}\right)^2-\left(\frac{\lambda_{1B}\lambda_{2B}}{\lambda_{1Bm}^i\lambda_{2Bm}^i}\right)^{-2}+3}.
\end{aligned} \tag{3.16}$$

Furthermore, the inelastic stretch ratios for each polymer subnetwork must satisfy the thermodynamic evolution law as presented by Reese and Govindjee (1998). For example, for membrane A,

$$-\frac{1}{2}\mathbf{F}_A\frac{d\left[\left(\mathbf{C}_{Am}^i\right)^{-1}\right]}{dt}\mathbf{F}_A^T\left(\mathbf{b}_{Am}^e\right)^{-1}=\boldsymbol{\gamma}^{-1}{}_m:\sigma_m^{NEQ}, \tag{3.17}$$

with $\mathbf{C}_{Am}^i=\left(\mathbf{F}_{Am}^i\right)^T\mathbf{F}_{Am}^i$, $\mathbf{C}_{Am}^e=\left(\mathbf{F}_{Am}^e\right)^T\mathbf{F}_{Am}^e$, $\mathbf{b}^e{}_m=\mathbf{F}_{Am}^e\left(\mathbf{F}_{Am}^e\right)^T$, and $\sigma_m^{NEQ}=2\mathbf{F}_{Am}^e\frac{\partial W^{NEQ}{}_m}{\partial\mathbf{C}_{Am}^e}\left(\mathbf{F}_{Am}^e\right)^T$. The isotropic rank-four mobility tensor $\boldsymbol{\gamma}^{-1}{}_m$ must be positive-definite to meet Eq. (3.17), and it takes the expression as follows

$$\boldsymbol{\gamma}^{-1}{}_m=\frac{1}{2\eta_{Dm}}\left(\mathbf{I}^4-\frac{1}{3}\mathbf{I}\otimes\mathbf{I}\right), \tag{3.18}$$

where η_{Dm} is the shear viscosity of each polymer subnetwork, $\mathbf{I}^4$ is the fourth order symmetric identity tensor and $\mathbf{I}$ is the second order identity tensor. With Eq. (3.17) and (3.18), we can obtain the inelastic stretch ratios of each polymer subnetwork of membrane A, i.e.,

$$\frac{d\lambda_{1Am}^{i}}{dt}=\tau_m\frac{J_{\lim}\lambda_{1Am}^{i}}{6\left[J_{\lim}-\left(\frac{\lambda_{1A}}{\lambda_{1Am}^{i}}\right)^2-\left(\frac{\lambda_{2p}}{\lambda_{2Am}^{i}}\right)^2-\left(\frac{\lambda_{1A}}{\lambda_{1Am}^{i}}\frac{\lambda_{2p}}{\lambda_{2Am}^{i}}\right)^{-2}+3\right]}\left[2\left(\frac{\lambda_{1A}}{\lambda_{1Am}^{i}}\right)^2-\left(\frac{\lambda_{2p}}{\lambda_{2Am}^{i}}\right)^2-\left(\frac{\lambda_{1A}\lambda_{2p}}{\lambda_{1Am}^{i}\lambda_{2Am}^{i}}\right)^{-2}\right], \tag{3.19}$$

$$\frac{d\lambda_{2Am}^{i}}{dt}=\tau_m\frac{J_{\lim}\lambda_{2Am}^{i}}{6\left[J_{\lim}-\left(\frac{\lambda_{1A}}{\lambda_{1Am}^{i}}\right)^2-\left(\frac{\lambda_{2p}}{\lambda_{2Am}^{i}}\right)^2-\left(\frac{\lambda_{1A}}{\lambda_{1Am}^{i}}\frac{\lambda_{2p}}{\lambda_{2Am}^{i}}\right)^{-2}+3\right]}\left[2\left(\frac{\lambda_{2p}}{\lambda_{2Am}^{i}}\right)^2-\left(\frac{\lambda_{1A}}{\lambda_{1Am}^{i}}\right)^2-\left(\frac{\lambda_{1A}\lambda_{2p}}{\lambda_{1Am}^{i}\lambda_{2Am}^{i}}\right)^{-2}\right], \tag{3.20}$$

where $\tau_m = G^{NEQ}{}_m / \eta_{Dm}$ represents the relaxation time of each polymer subnetwork of the DE membrane. Similarly, the time-dependent inelastic stretch ratios of each polymer subnetwork of membrane B can be obtained as

$$\frac{d\lambda_{1Bm}^{i}}{dt}=\tau_m\frac{J_{\lim}\lambda_{1Bm}^{i}}{6\left[J_{\lim}-\left(\frac{\lambda_{1B}}{\lambda_{1Bm}^{i}}\right)^2-\left(\frac{\lambda_{2p}}{\lambda_{2Bm}^{i}}\right)^2-\left(\frac{\lambda_{1B}}{\lambda_{1Bm}^{i}}\frac{\lambda_{2p}}{\lambda_{2Bm}^{i}}\right)^{-2}+3\right]}\left[2\left(\frac{\lambda_{1B}}{\lambda_{1Bm}^{i}}\right)^2-\left(\frac{\lambda_{2p}}{\lambda_{2Bm}^{i}}\right)^2-\left(\frac{\lambda_{1B}\lambda_{2p}}{\lambda_{1Bm}^{i}\lambda_{2Bm}^{i}}\right)^{-2}\right], \tag{3.21}$$

$$\frac{d\lambda_{2Bm}^{i}}{dt}=\tau_m\frac{J_{\lim}\lambda_{2Bm}^{i}}{6\left[J_{\lim}-\left(\frac{\lambda_{1B}}{\lambda_{1Bm}^{i}}\right)^2-\left(\frac{\lambda_{2p}}{\lambda_{2Bm}^{i}}\right)^2-\left(\frac{\lambda_{1B}}{\lambda_{1Bm}^{i}}\frac{\lambda_{2p}}{\lambda_{2Bm}^{i}}\right)^{-2}+3\right]}\left[2\left(\frac{\lambda_{2p}}{\lambda_{2Bm}^{i}}\right)^2-\left(\frac{\lambda_{1B}}{\lambda_{1Bm}^{i}}\right)^2-\left(\frac{\lambda_{1B}\lambda_{2p}}{\lambda_{1Bm}^{i}\lambda_{2Bm}^{i}}\right)^{-2}\right]. \tag{3.22}$$

Since the thickness L_3 of the membrane of the resonator is much less than the lengths ($L_3 \ll L_1, L_2$), the resonator cannot sustain compression during the operation. Therefore, the stresses of membranes in both directions need to be ensured to be positive, i.e., $P_{1A}/GL_2L_3 > 0$, $P_{2A}/GL_AL_3 > 0$, $P_{1B}/GL_2L_3 > 0$, and $P_{2B}/GL_BL_3 > 0$. Besides, when the electric field induced by the voltage applied to the membrane A exceeds the dielectric strength E_{EB}, the resonator fails by electric breakdown. The critical applied voltage V_{EB} can be determined as (Koh *et al*., 2011; Zhou *et al*., 2013)

$$\frac{V_{EB}}{L_3}\sqrt{\frac{\varepsilon\varepsilon_0}{G}} = d(\lambda_{1A}\lambda_{2A})^{-1}, \tag{3.23}$$

with the material parameter $d = E_{EB}\sqrt{\varepsilon\varepsilon_0/G}$. We choose a moderate value of d=5 for the following simulation (Koh et al., 2011).

3.3 Natural frequency of the DE Membrane Resonator

Combining Eq. (3.11), (3.13) and Eq. (3.15) with geometric relations $\lambda_{1B} = \lambda_{1p} + k\left(\lambda_{1p} - \lambda_{1A}\right)$, and $\lambda_{2A} = \lambda_{2B} = \lambda_{2p}$, we get the motion equation for the rigid bars as

$$\frac{d^2\lambda_{1A}}{dt^2} + g\left(\lambda_{1A}, \lambda_{1Am}^i, \lambda_{2Am}^i, \lambda_{1Bm}^i, \lambda_{2Bm}^i, V_A\right) = 0, \tag{3.24}$$

with

$$g\left(\lambda_{1A},\lambda_{1Am}^{i},\lambda_{2Am}^{i},\lambda_{1Bm}^{i},\lambda_{2Bm}^{i},V_A\right)$$
$$=\alpha\{\frac{\chi J_{\lim}\left(\lambda_{1A}-\lambda_{1A}^{-3}\lambda_{2p}^{-2}\right)}{J_{\lim}-\lambda_{1A}^{2}-\lambda_{2p}^{2}-\lambda_{1A}^{-2}\lambda_{2p}^{-2}+3}+\sum_{m=1}^{n}\frac{G^{NEQ}{}_{m}}{G}\frac{J_{\lim}\left[\lambda_{1A}\lambda_{1A}^{i-2}{}_{m}-\lambda_{1A}^{-3}\lambda_{2p}^{-2}\left(\lambda_{1Am}^{i}\lambda_{2Am}^{i}\right)^{2}\right]}{J_{\lim}-\left(\frac{\lambda_{1A}}{\lambda_{1Am}^{i}}\right)^{2}-\left(\frac{\lambda_{2p}}{\lambda_{2Am}^{i}}\right)^{2}-\left(\frac{\lambda_{1A}\lambda_{2p}}{\lambda_{1Am}^{i}\lambda_{2Am}^{i}}\right)^{-2}+3}$$
$$-\frac{\chi J_{\lim}\left(\lambda_{1B}-\lambda_{1B}^{-3}\lambda_{2p}^{-2}\right)}{J_{\lim}-\lambda_{1B}^{2}-\lambda_{2p}^{2}-\lambda_{1B}^{-2}\lambda_{2p}^{-2}+3}-\sum_{m=1}^{n}\frac{G^{NEQ}{}_{m}}{G}\frac{J_{\lim}\left[\lambda_{1B}\lambda_{1B}^{i-2}{}_{m}-\lambda_{1B}^{-3}\lambda_{2p}^{-2}\left(\lambda_{1Bm}^{i}\lambda_{2Bm}^{i}\right)^{2}\right]}{J_{\lim}-\left(\frac{\lambda_{1B}}{\lambda_{1Bm}^{i}}\right)^{2}-\left(\frac{\lambda_{2p}}{\lambda_{2Bm}^{i}}\right)^{2}-\left(\frac{\lambda_{1B}\lambda_{2p}}{\lambda_{1Bm}^{i}\lambda_{2Bm}^{i}}\right)^{-2}+3}$$
$$-\frac{\varepsilon\varepsilon_0}{G}\left(\frac{V_A}{L_3}\right)^{2}\lambda_{1A}\lambda_{2p}^{2}\}$$

and $\alpha=1/\left(\frac{L_{1A}^{2}}{3G}\rho-\frac{L_{1B}^{2}}{3G}k\rho+\frac{mL_{1A}}{GL_2L_3}\right)$.

To find the natural frequency ω_n, we follow the previous studies (Zhu et al., 2010; Li et al., 2012; Zhang et al., 2014a and 2014b) regarding the nonlinear vibration analysis for viscoelastic DE oscillators. At any time, *t*, when a small amplitude $\Delta(t)$ of perturbation is applied in 1-direction to the rigid bars, the induced deformation of membrane A is

$$\lambda_{1A}(t)=\lambda_{1A}'+\Delta(t), \tag{3.25}$$

with $\lambda_{1A}'=\lambda_{1A}$ being the stretch ratio of membrane A before the perturbation is applied. Expanding the function $g\left(\lambda_{1A},\lambda_{1Am}^{i},\lambda_{2Am}^{i},\lambda_{1Bm}^{i},\lambda_{2Bm}^{i},V_A\right)$ into the first order Taylor series in terms of $\Delta(t)$ gives

$$g\left(\lambda_{1A},\lambda_{1Am}^{i},\lambda_{2Am}^{i},\lambda_{1Bm}^{i},\lambda_{2Bm}^{i},V_A\right)$$
$$=g\left(\lambda_{1A}',\lambda_{1Am}^{i},\lambda_{2Am}^{i},\lambda_{1Bm}^{i},\lambda_{2Bm}^{i},V_A\right)+\frac{\partial g\left(\lambda_{1A}',\lambda_{1Am}^{i},\lambda_{2Am}^{i},\lambda_{1Bm}^{i},\lambda_{2Bm}^{i},V_A\right)}{\partial\lambda_{1A}}\Delta \tag{3.26}$$

Combining Eqs. (3.24) ~ (3.26), we obtain the motion equation in terms of perturbation $\Delta(t)$, i.e.,

$$\frac{d^2\Delta}{dt^2}+\frac{\partial g\left(\lambda'_{1A},\lambda^i_{1Am},\lambda^i_{2Am},\lambda^i_{1Bm},\lambda^i_{2Bm},V_A\right)}{\partial\lambda_{1A}}\Delta=0. \tag{3.27}$$

Then the natural frequency of the DE resonator can be expressed as

$$\omega_n^2=\frac{\partial g\left(\lambda'_{1A},\lambda^i_{1Am},\lambda^i_{2Am},\lambda^i_{1Bm},\lambda^i_{2Bm},V_A\right)}{\partial\lambda_{1A}}. \tag{3.28}$$

Combining Eqs. (3.24) and (3.28), we obtain the natural frequency as

$$\omega_n^2 = \alpha\{\frac{\chi J_{\lim}\left(1+3\lambda_{1A}^{-4}\lambda_{2p}^{-2}\right)}{J_{\lim}-\lambda_{1A}^2-\lambda_{2p}^2-\lambda_{1A}^{-2}\lambda_{2p}^{-2}+3}+\frac{2\chi J_{\lim}\left(\lambda_{1A}-\lambda_{1A}^{-3}\lambda_{2p}^{-2}\right)^2}{\left(J_{\lim}-\lambda_{1A}^2-\lambda_{2p}^2-\lambda_{1A}^{-2}\lambda_{2p}^{-2}+3\right)^2}$$

$$+\sum_{m=1}^{n}\frac{G^{NEQ}{}_m}{G}\frac{J_{\lim}\left[\lambda_{1A}^{i-2}{}_m+3\lambda_{1A}^{-4}\lambda_{2p}^{-2}\left(\lambda_{1Am}^i\lambda_{2Am}^i\right)^2\right]}{J_{\lim}-\left(\frac{\lambda_{1A}}{\lambda_{1Am}^i}\right)^2-\left(\frac{\lambda_{2p}}{\lambda_{2Am}^i}\right)^2-\left(\frac{\lambda_{1A}\lambda_{2p}}{\lambda_{1Am}^i\lambda_{2Am}^i}\right)^{-2}+3}$$

$$+\sum_{m=1}^{n}\frac{G^{NEQ}{}_m}{G}\frac{2J_{\lim}\left[\lambda_{1A}\lambda_{1A}^{i-2}{}_m-\lambda_{1A}^{-3}\lambda_{2p}^{-2}\left(\lambda_{1Am}^{i2}\lambda_{2Am}^{i2}\right)^2\right]^2}{\left[J_{\lim}-\left(\frac{\lambda_{1A}}{\lambda_{1Am}^i}\right)^2-\left(\frac{\lambda_{2p}}{\lambda_{2Am}^i}\right)^2-\left(\frac{\lambda_{1A}\lambda_{2p}}{\lambda_{1Am}^i\lambda_{2Am}^i}\right)^{-2}+3\right]^2}$$

$$+\frac{k\chi J_{\lim}\left\{1+3\lambda_{2p}^{-2}\lambda_{1B}^{-4}\right\}}{J_{\lim}-\lambda_{1B}^2-\lambda_{2p}^2-\left[\lambda_{1p}+\alpha\left(\lambda_{1p}-\lambda_{1A}\right)\right]^{-2}\lambda_{2p}^{-2}+3}$$

$$+\frac{2k\chi J_{\lim}\left\{\left[\lambda_{1p}+\alpha\left(\lambda_{1p}-\lambda_{1A}\right)\right]-\lambda_{2p}^{-2}\left[\lambda_{1p}+\alpha\left(\lambda_{1p}-\lambda_{1A}\right)\right]^{-3}\right\}^2}{\left\{J_{\lim}-\left[\lambda_{1p}+\alpha\left(\lambda_{1p}-\lambda_{1A}\right)\right]^2-\lambda_{2p}^2-\left[\lambda_{1p}+\alpha\left(\lambda_{1p}-\lambda_{1A}\right)\right]^{-2}\lambda_{2p}^{-2}+3\right\}^2}$$

$$+\sum_{m=1}^{n}\frac{G^{NEQ}{}_m}{G}\frac{kJ_{\lim}\left\{\lambda_{1B}^{i-2}{}_m+3\lambda_{2p}^{-2}\left(\lambda_{1Bm}^i\lambda_{2Bm}^i\right)^2\left[\lambda_{1p}+\alpha\left(\lambda_{1p}-\lambda_{1A}\right)\right]^{-4}\right\}}{J_{\lim}-\left[\frac{\lambda_{1p}+\alpha\left(\lambda_{1p}-\lambda_{1A}\right)}{\lambda_{1Bm}^i}\right]^2-\left(\frac{\lambda_{2p}}{\lambda_{2Bm}^i}\right)^2-\left\{\frac{\left[\lambda_{1p}+\alpha\left(\lambda_{1p}-\lambda_{1A}\right)\right]\lambda_{2p}}{\lambda_{1Bm}^i\lambda_{2Bm}^i}\right\}^{-2}+3}$$

$$+\sum_{m=1}^{n}\frac{G^{NEQ}{}_m}{G}\frac{2kJ_{\lim}\left\{\left[\lambda_{1p}+\alpha\left(\lambda_{1p}-\lambda_{1A}\right)\right]\lambda_{1B}^{i-2}{}_m-\lambda_{2p}^{-2}\left(\lambda_{1Bm}^i\lambda_{2Bm}^i\right)^2\left[\lambda_{1p}+\alpha\left(\lambda_{1p}-\lambda_{1A}\right)\right]^{-3}\right\}^2}{\left\{J_{\lim}-\left[\frac{\lambda_{1p}+\alpha\left(\lambda_{1p}-\lambda_{1A}\right)}{\lambda_{1Bm}^i}\right]^2-\left(\frac{\lambda_{2p}}{\lambda_{2Bm}^i}\right)^2-\left\{\frac{\left[\lambda_{1p}+\alpha\left(\lambda_{1p}-\lambda_{1A}\right)\right]\lambda_{2p}}{\lambda_{1Bm}^i\lambda_{2Bm}^i}\right\}^{-2}+3\right\}^2}$$

$$-\frac{\varepsilon\varepsilon_0}{G}\left(\frac{V_A}{L_3}\right)^2\lambda_{2p}^2\}. \tag{3.29}$$

From Eq. 3.29, it is clear that the natural frequency of the resonator depends on the relaxation time of each polymer subnetwork, as well as the total number *n* of polymer subnetworks. When the geometric and material parameters are given, the natural frequency

can be obtained by solving equations (3.16), (3.19), (3.20), (3.21), (3.22) and (3.29), the ordinary differential equations are solved by ODE15s function in MATLAB.

3.4 Simulation Results and Discussion

In order to illustrate the actuation process and natural frequency tuning of the DE membrane resonator, we first consider the case in which the voltage is applied instantaneously to membrane A with a loading rate $r = dV^* / dt$ after pre-stretching, framing and clamping of the DE membrane (before it starts to relax). The dimensionless voltage is defined as $V^* = V\sqrt{\varepsilon\varepsilon_0 / G} / L_3$, and the length ratio and the pre-stretch ratios are set as k = 1, λ_{1p} = 2 and λ_{2p} = 4, respectively. The typical electromechanical response of the resonator ($\lambda_{1A} - V^*$) with different values of viscoelastic material parameter χ is plotted in Figure 3.2, in which $\chi = G^{EQ}/G$ is selected as 0.1, 0.5 and 0.9, respectively. The dimensionless voltage V^* on membrane A is increased at a loading rate r=0.3 until the loss-of-tension of the membrane either in 1-direction (denoted by triangle) or 2-direction (denoted by rectangle). For the model of a single polymer subnetwork (dotted lines), the relaxation time is chosen as τ =1s, while the three relaxation times are assumed as τ =0.01s, 1s, 100s for the model with three polymer subnetworks (solid lines). With the same conditions and the loading process, figure 3.3 shows the dimensionless natrual frequency $\Omega_n = \omega_n / \sqrt{\alpha}$ as a function of the dimensionless applied voltage V^*.

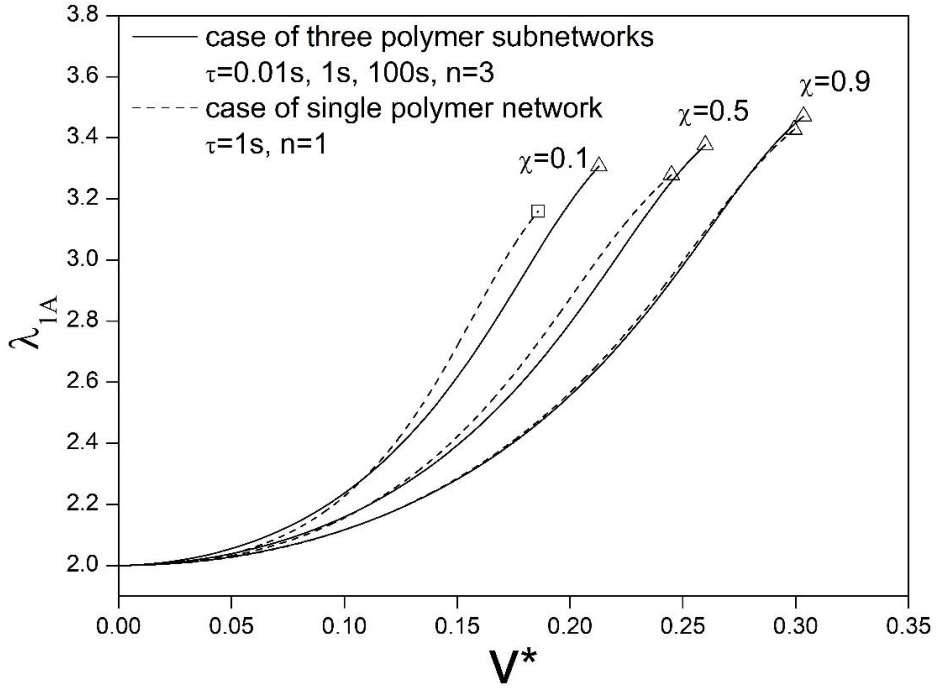

Figure 3.2 Electromechanical response (λ_{1A} Vs. V^*) of DE membrane resonators with single polymer subnetwork τ =1s, n=1 (dotted lines), and three polymer subnetworks τ = 0.01s, 1s, 100s, n=3 (solid lines), χ = 0.1, 0.5, 0.9, respectively, at r = 0.3, α=1, λ_{1p}=2, λ_{2p}=4.

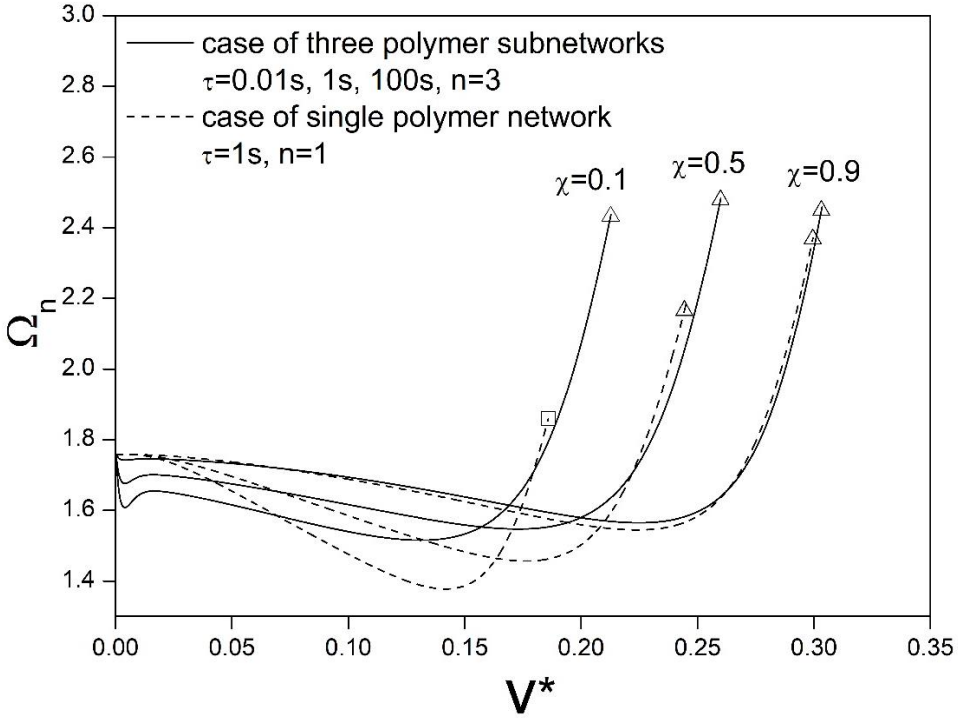

Figure 3.3 Dimensionless natural frequency response (Ω_n Vs. V^*) of DE membrane resonators with single polymer subnetwork τ =1s, n=1 (dotted lines), and three polymer subnetworks τ =0.01s, 1s, 100s, n=3 (solid lines), χ =0.1, 0.5, 0.9, respectively, at r=0.3, α=1, λ_{1p}=2, λ_{2p}=4.

It shows that the stretch ratio increases monotonically for both cases, while the natural frequency changes non-monotonically as the applied voltage increases. The non-monotonic behavior observed in figure 3.3 may be linked to the change of the stiffness of the membrane during the actuation (indicated by the slope of stretch ratio curves in figure 3.2). In general, it is observed from figure 3.2 that the DE modeled with three polymer subnetworks can sustain a higher voltage, i.e., the loss-of-tesnison failure of the membrane is delayed. Correspondingly, larger deformation of the membrane and higher natural frequency tuned by the applied voltage could be achieved. For the DE model with a single polymer subnetwork, the stiffness of the membrane decresease for small voltage, then increases as the applied voltage increases. The natural frequency of the membrane tuned by the voltage thus drops with the increase of the voltage and then rises up as the voltage continues to increase. A localized minimum natural frequency could be achieved. However, for the DE model with three polymer subnetworks, the variation of the stiffness of the membrane is more complex due to the interaction of the subnetworks. The variation of the membrane stiffness is caused by the stress relaxation and the electromechanical coupling for a viscoelastic DE. It should be mentioned that with the increase of χ, the results for the two different models become closer. This is expected since the response of the membrane is mainly governed by the purely elastic ground network for this condition. From Fig. 3.2 and and Fig. 3.3, it is concluded that both the material parameter χ and the polymer subnetworks strongly affect the actuation response and the frequency tuning of the DE resonator. Particularly, for the material possessing lower fraction of elastic ground network, it is more adjustable to tune the resonator frequency by tailoring the polymer subnetworks.

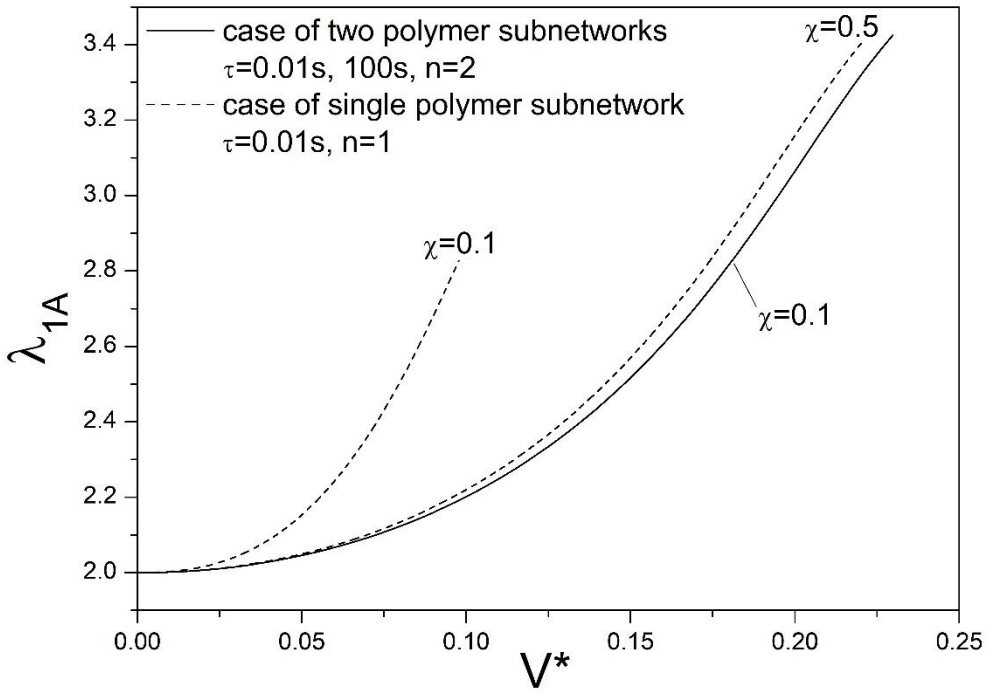

Figure 3.4 Electromechanical response (λ_{1A} Vs. V^*) of DE membrane resonators with a single polymer subnetwork τ =0.01s, χ =0.1, 0.5, respectively; and two polymer subnetworks τ =0.01s, 100s, n=2, χ =0.1, at r=0.3, k=1, λ_{1p}=2, λ_{2p}=4.

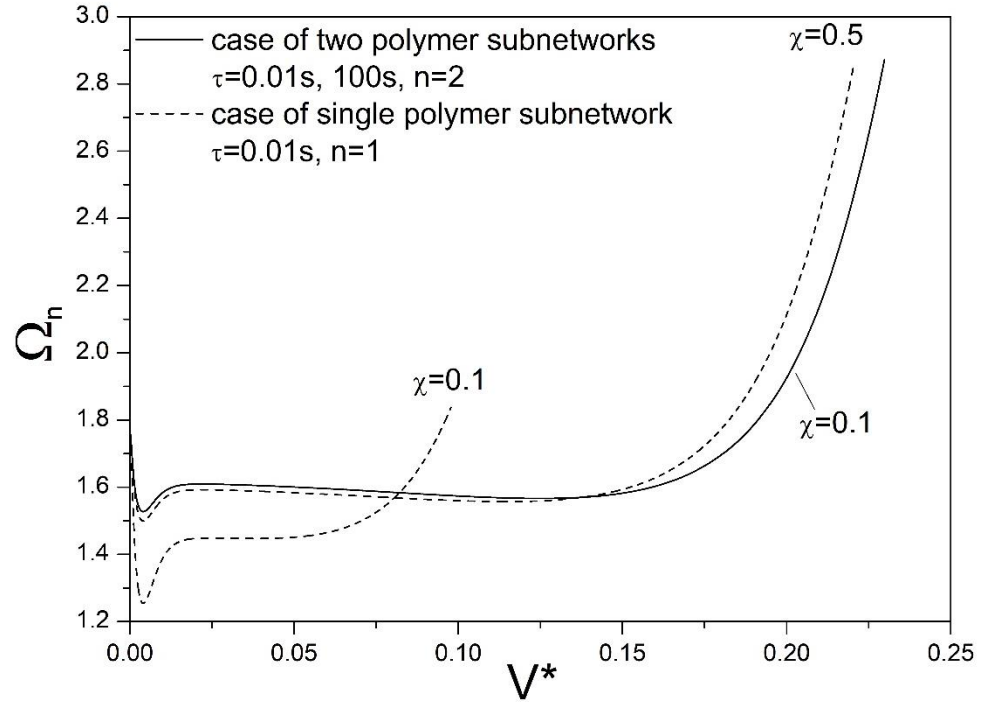

Figure 3.5 Dimensionless natural frequency response (Ω_n Vs. V^*) of DE membrane resonators with a single polymer subnetwork τ =0.01s, χ =0.1, 0.5, respectively; and two polymer subnetworks τ =0.01s, 100s, n=2, χ =0.1, at r=0.3, k=1, λ_{1p}=2, λ_{2p}=4.

Fig. 3.4 shows a comparison of the combined effects of χ and the polymer subnetworks on the actuation response. For the material with the same polymer subnetwork, for example, n=1 and τ=0.01 s, with a higher value of χ, the DE membrane can sustain a higher voltage, which leads to a larger deformation. For the material with different fraction of purely elastic ground network, i.e., the value of χ, it is also possible to achieve the similar actuation response by adding some other polymer subnetworks. As demonstrated in Fig. 3.4, when one polymer subnetwork with a relaxation time of τ=100 s is added into the DE with the original polymer subnetwork of a relaxation time of τ=0.01 s, the materials with different fraction of the purely elastic ground network respond in a similar way. Since the two electromechanical response curves are rather close to each other, the frequency tuning processes are also similar, as shown in Fig. 3.5. Furthermore, the results stay similar as well when the electric loading is changed into a relatively high rate as shown in Fig. 3.6 and Fig. 3.7. It is concluded that the electromechanical response and frequency tuning could be modified by tailoring the microstructure of the DE material.

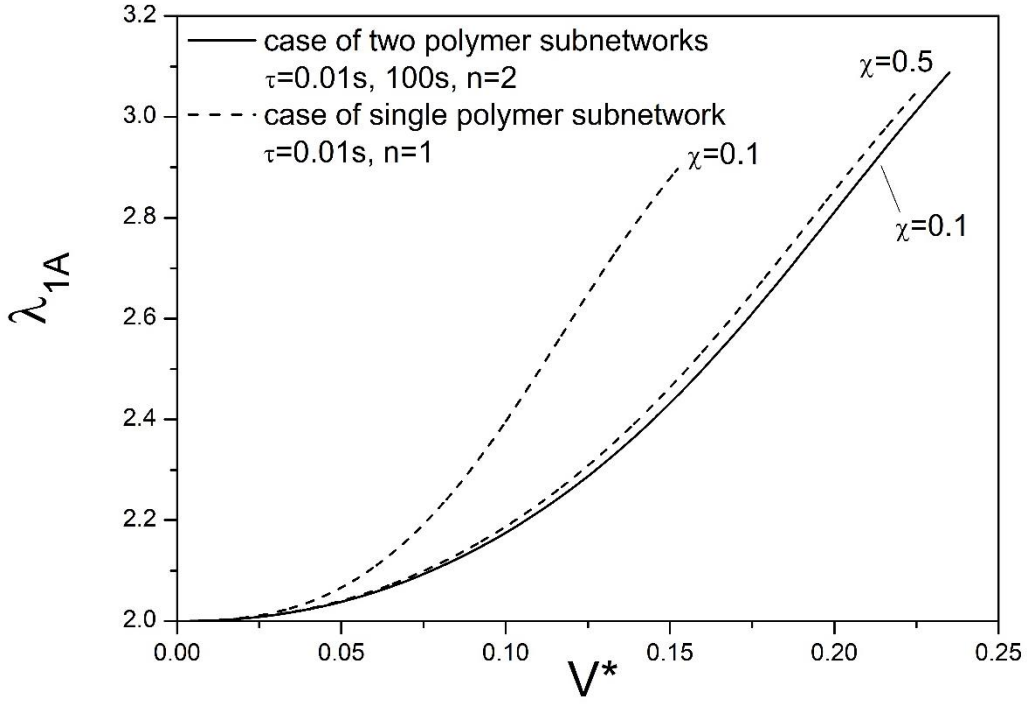

Figure 3.6 Electromechanical response (λ_{1A} Vs. V^*) of DE membrane resonators with a single polymer subnetwork τ =0.01s, χ =0.1, 0.5, respectively; and two polymer subnetworks τ =0.01s, 100s, n=2, χ =0.1, at r=10, k=1, λ_{1p}=2, λ_{2p}=4.

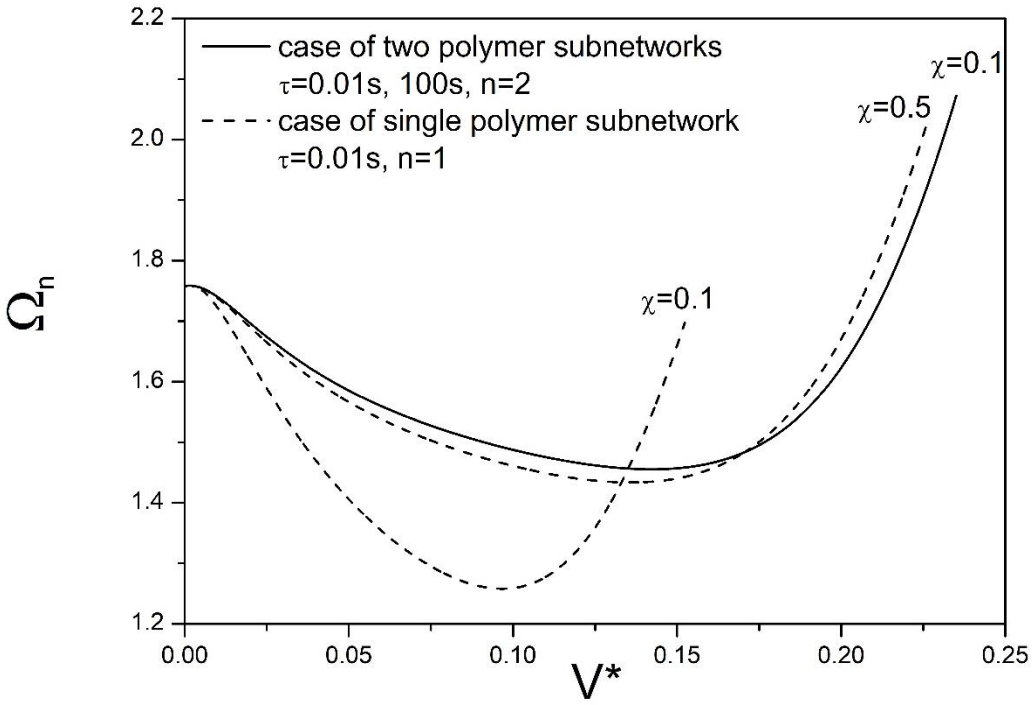

Figure 3.7 Dimensionless natural frequency response (Ω_n Vs. V^*) of DE membrane resonators with single polymer subnetwork τ =0.01s, χ =0.1, 0.5, respectively; and two polymer subnetworks τ =0.01s, 100s, n=2, χ =0.1, at r=10, k=1, λ_{1p}=2, λ_{2p}=4.

Fig. 3.4 and Fig. 3.5 demonstrate the effect of adding a polymer subnetwork with longer relaxation time (τ=100 s) to the elastomer. On the other hand, Fig. 3.8 shows the effect of adding a polymer subnetwork with shorter relaxation time (τ=0.01 s) on the actuation response of the DE. The DE with a single polymer subnetwork withstands a higher critical voltage, as well as a larger deformation. Moreover, its actuation response is insensitive to the material viscosity χ when the applied voltage rate is relatively high (r=10), while the response of the DE with two polymer subnetworks is still significantly affected by χ. The same effect on corresponding frequency tuning processes is shown as well in Fig. 3.9.

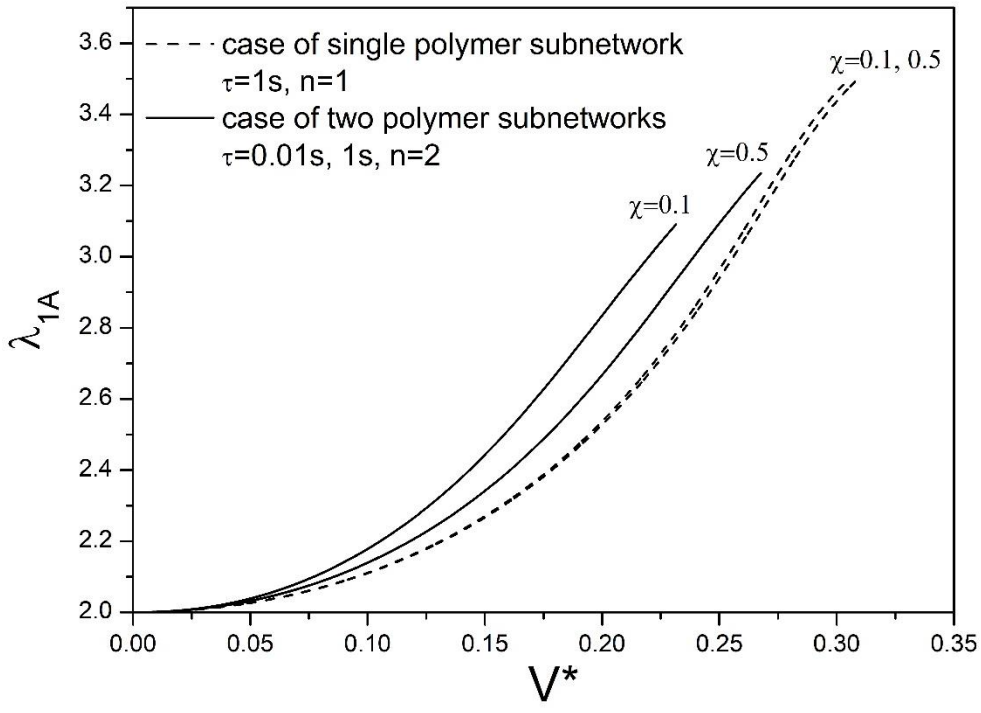

Figure 3.8 Electromechanical response (λ_{1A} Vs. V^*) of DE membrane resonators with single polymer subnetwork τ=0.01s, n=1; and two polymer subnetworks τ=0.01s, 1s,

n=2; for χ=0.1, 0.5, respectively, and *k* =1, λ_{1p} =2, λ_{2p} =4. The voltage rate is applied at r= 10.

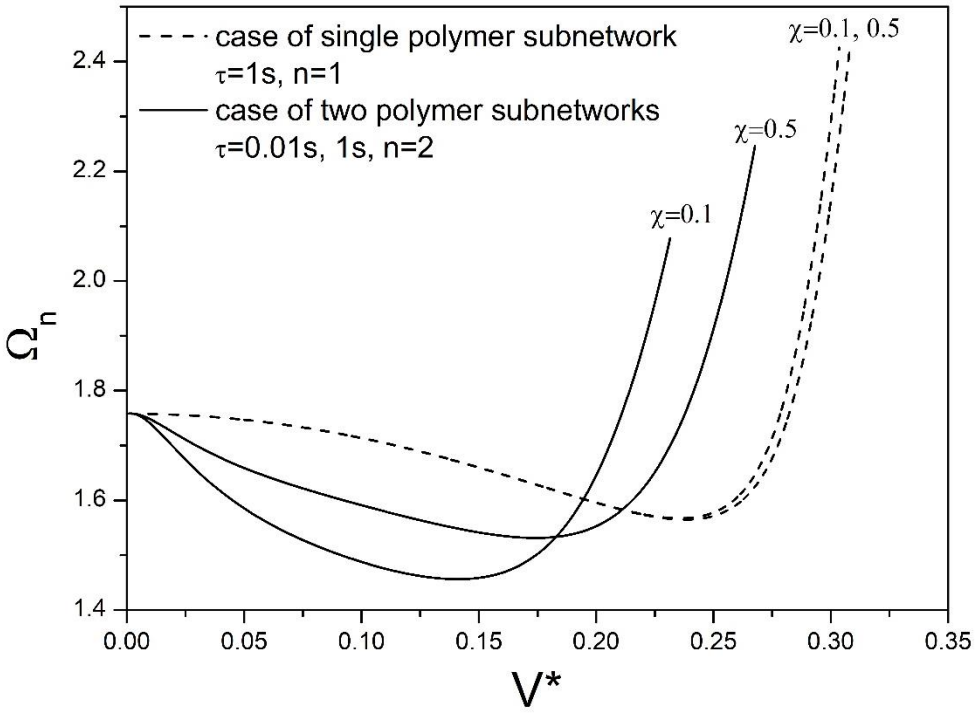

Figure 3.9 Dimensionless natural frequency response (Ω_n Vs. V^*) of DE membrane resonators with single polymer subnetwork τ =0.01s, n=1; and two polymer subnetworks τ =0.01s, 1s, n=2; for χ =0.1, 0.5, respectively, and *k* =1, λ_{1p} =2, λ_{2p} =4. The voltage rate is applied at r= 10.

For Figures 3.2-3.9, the voltage is applied before the DE mambrane starts to relax. However, in many DE-based applications, the voltage is very likely to be applied after the DE membrane is completely relaxed. Therefore, Fig. 3.10 illustrates the the tuning process of the dimensionless natural frequency under the circumstance that the voltage is applied on a fully relaxed DE. The voltage rate, the length ratio, the pre-stretch ratios and the material parameter χ are set as r =0.3, k = 1, λ_{1p} = 2, λ_{2p} = 4, and χ =0.5, respectively. For the case of a single polymer subnetwork (dotted lines), the relaxation time is chosen as τ =100s, while the relaxation times of the three subnetworks are set as τ =0.01 s, 1 s, 100 s (solid lines).

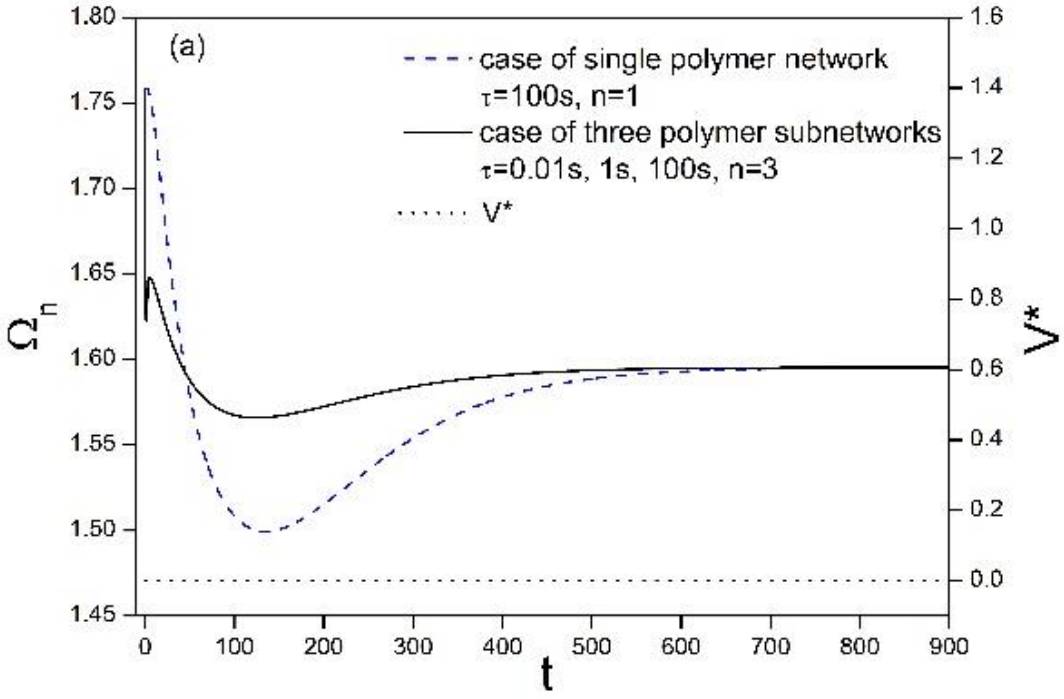
(a)
case of single polymer network
τ=100s, n=1
case of three polymer subnetworks
τ=0.01s, 1s, 100s, n=3
V*
Ω_n
V*
t
1.80
1.75
1.70
1.65
1.60
1.55
1.50
1.45
1.6
1.4
1.2
1.0
0.8
0.6
0.4
0.2
0.0
0
100
200
300
400
500
600
700
800
900

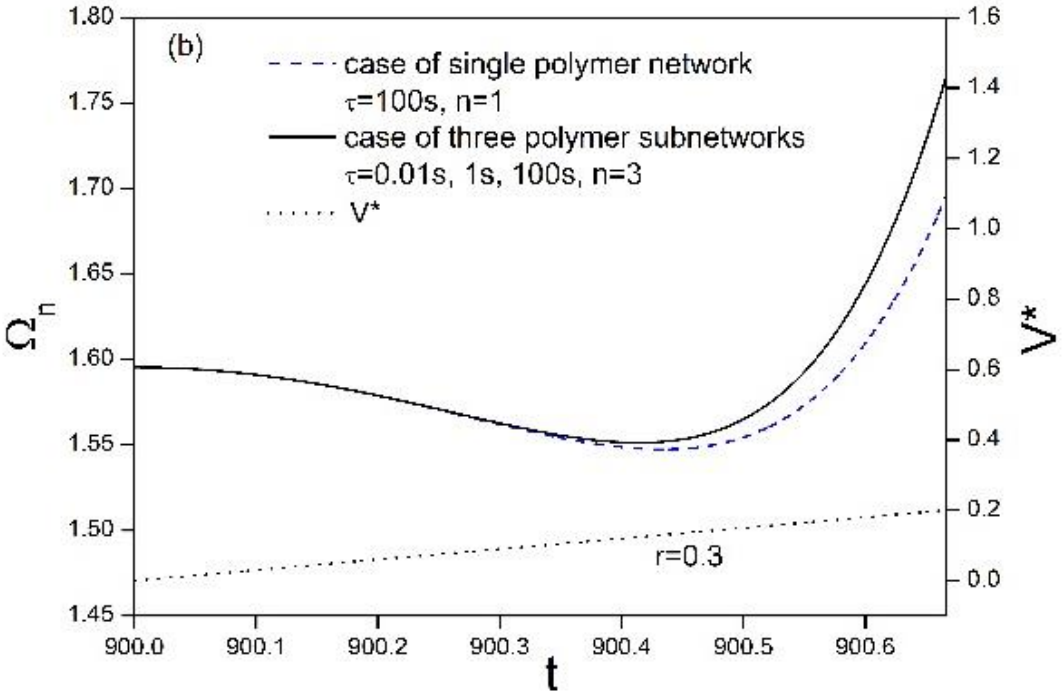
(b)
case of single polymer network
τ=100s, n=1
case of three polymer subnetworks
τ=0.01s, 1s, 100s, n=3
V*
r=0.3
Ω_n
V*
t
1.80
1.75
1.70
1.65
1.60
1.55
1.50
1.45
1.6
1.4
1.2
1.0
0.8
0.6
0.4
0.2
0.0
900.0
900.1
900.2
900.3
900.4
900.5
900.6

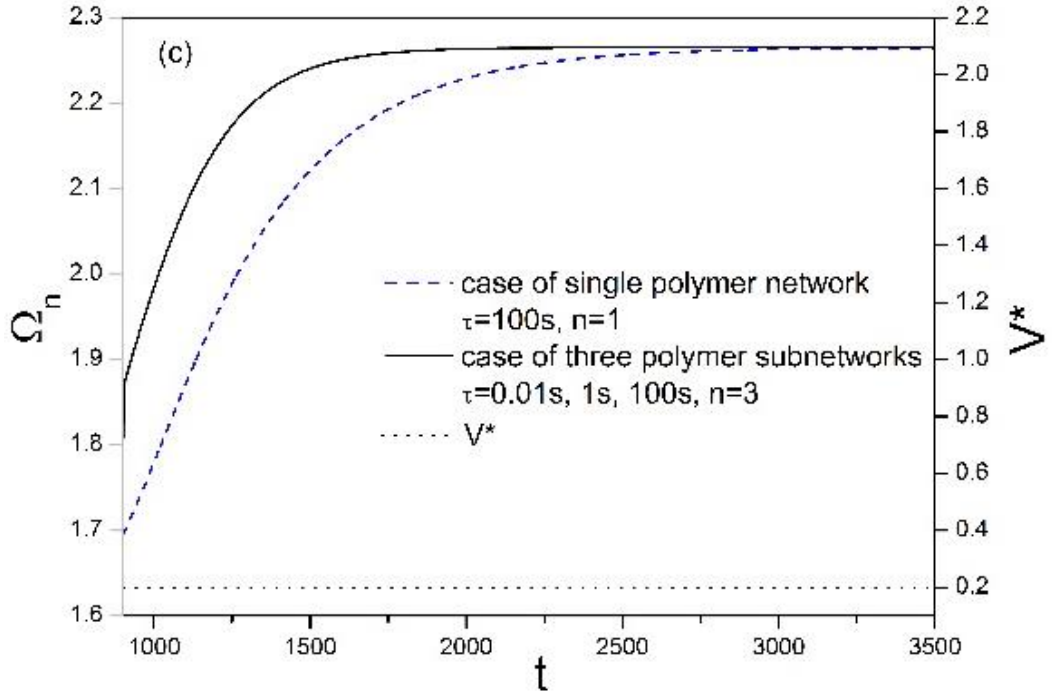
(c)
case of single polymer network
τ=100s, n=1
case of three polymer subnetworks
τ=0.01s, 1s, 100s, n=3
V*
Ω_n
V*
t

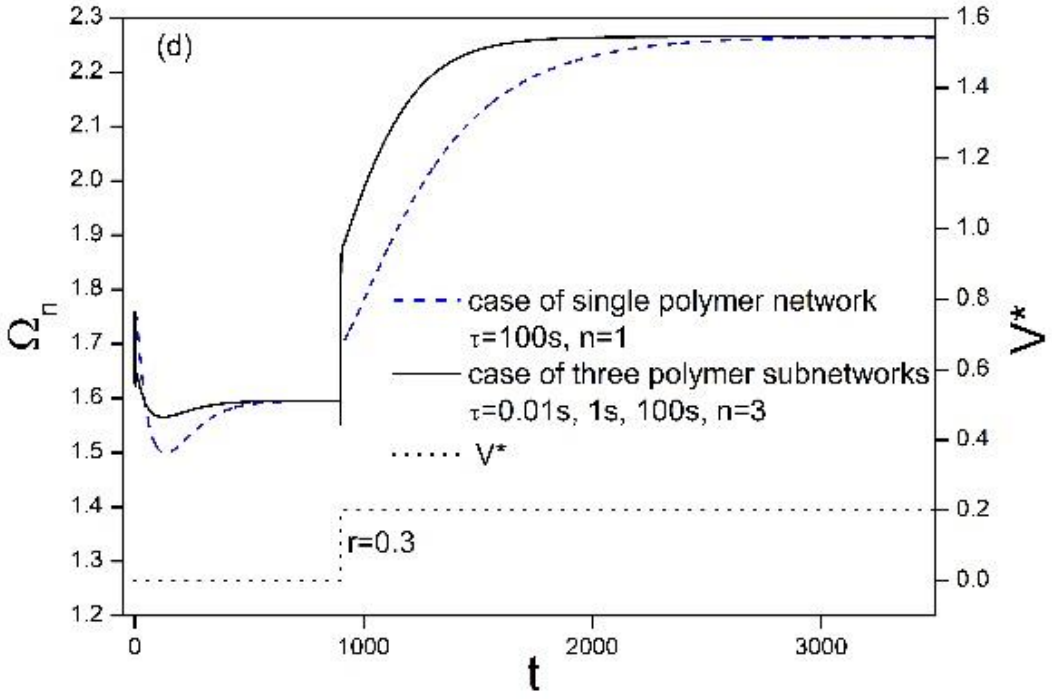
(d)
case of single polymer network
τ=100s, n=1
case of three polymer subnetworks
τ=0.01s, 1s, 100s, n=3
V*
r=0.3
Ω_n
V*
t

Figure 3.10 The natural frequency variation (Ω_n Vs. t) of DE membrane resonators with single polymer subnetwork τ=100 s, n=1 (dotted line); and three polymer subnetworks τ=0.01 s, 1 s, 100 s, n=3 (solid line), respectively, in the presence and absence of the applied voltage (stipple line), for χ=0.5, k =1, λ_{1p}=2, and λ_{2p}=4. (a) The preliminary stage for the polymer subnetworks to relax from the pre-stretching without voltage loading; (b) the actuation stage with voltage applied at the rate r=0.3; (c) the evolution stage with the constant voltage; (d) the complete natural frequency tuning process.

Fig. 3.10(a) describes the preliminary stage for the natural frequency tuning process of the DE membrane A, i.e., the relaxation without the applied voltage. Although the relaxtion process of the three subnetworks is a bit more complex than that of a single subnetwork, they both reach the same steady state in the end. For the actuation stage (Fig. 3.10(b)), after the membrane is fully relaxed, a voltage is applied at the rate of r =0.3 until it reaches the preset value $V_p^* = 0.2$, which is a safe value of the DE membrane. Since the DE is actuated by the applied voltage, the natural frequency first decreases and then increases. For the evolution stage (Fig. 3.10(c)), the applied voltage remains at V_p^*. Although the final steady state is the same for both cases, the DE with three subnetworks reaches it faster. The three stages for both cases are plotted in figure 3.10(d) to show the complete natural frequency tuning process. As can be seen from Fig. 3.10, once the DE is fully relaxed, the natrual frequency of both cases are the same. In fact, the number of polymer subnetworks does not affect the two steady states since they are only governed by the elastic ground network.

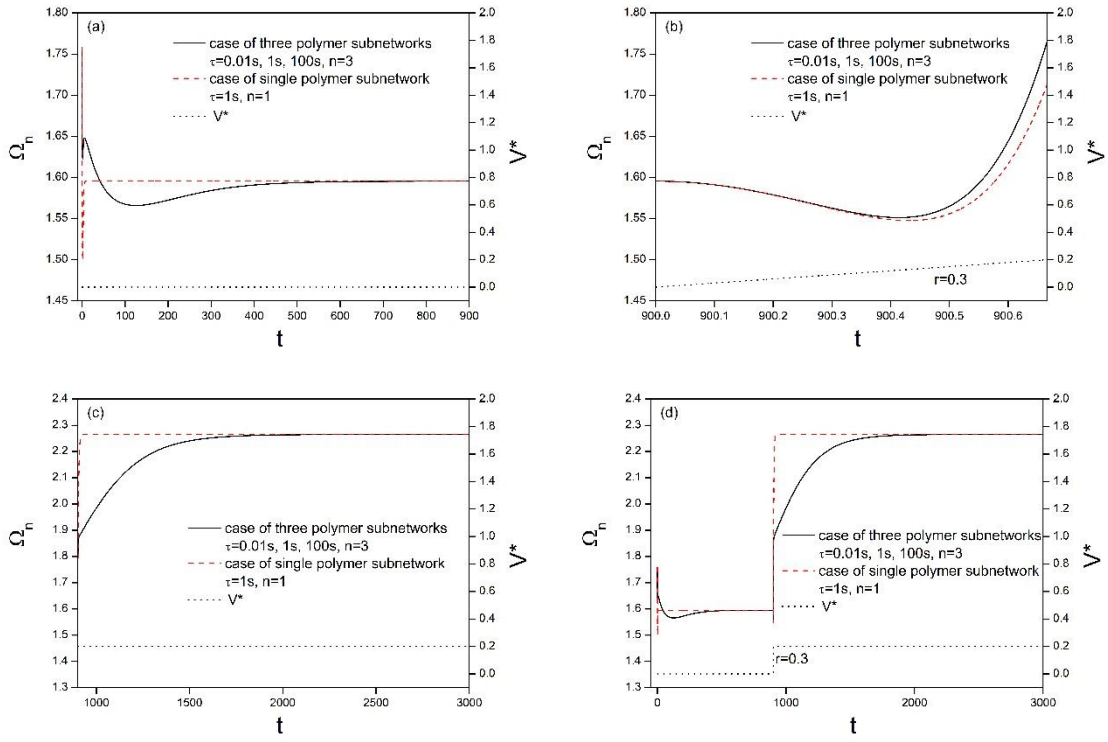

Figure 3.11 The natural frequency variation (Ω_n Vs. t) of DE membrane resonators with single polymer subnetwork τ =1 s, n=1 (dotted line); and three polymer subnetworks τ =0.01 s, 1 s, 100 s, n=3 (solid line), respectively, in the presence and absence of the applied voltage (stipple line), for χ =0.5, k =1, λ_{1p}=2, and λ_{2p}=4. (a) The preliminary stage; (b) the actuation stage; (c) the evolution stage; (d) the complete natural frequency tuning process.

Fig. 3.11 is the natural frequency tuning processes for the resonator of a single subnetwork with relaxation time τ =1 s, n=1, and the case of three subnetworks with τ =0.01 s, 1 s, 100 s, n=3. From Fig. 3.10 and Fig. 3.11, it concludes that although the natural frequency at steady states is independent of both the number and the relaxation time of polymer subnetworks, the time to achieve the steady states can be tuned obviously by tailoring the material polymer structure.

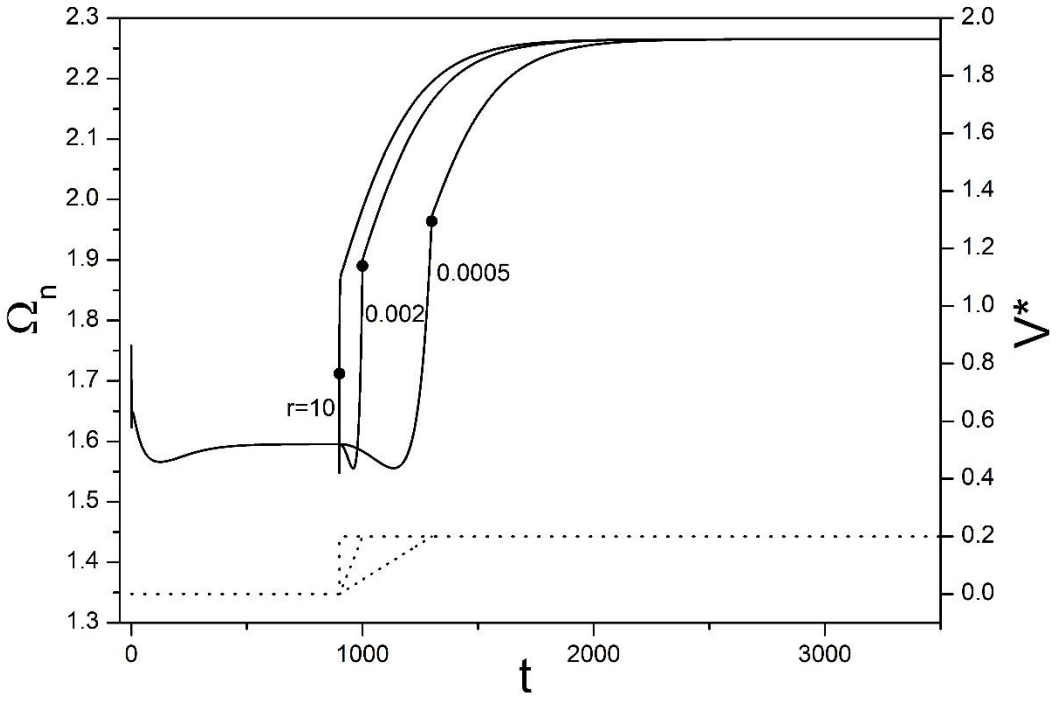

Figure 3.12 The complete natural frequency tuning process (Ω_n Vs. τ) of DE membrane resonators with three polymer subnetworks τ=0.01 s, 1 s, 100 s, n=3 (solid line), with voltage loadings(stipple line) applied at rates of r=10, 0.002, 0.0005, respectively, at the actuation stages, for χ=0.5, k =1, λ_{1p}=2, and λ_{2p}=4.

Fig. 3.12 depicts the effect of the loading rate of the applied voltage on the frequency tuning during the whole process. It can be seen that the rate of the applied voltage only affects the time that the DE takes to reach the final steady state, while it will not change the value of the steady natural frequency of the DE resonator. The pre-set voltage $V_p^* = 0.2$ in Figures 3.10 and 3.12 is a safe operation value that the DE membrane can reach the final steady state without any failure. In fact, the failure of the membrane (loss-of-tension or electrical breakdown) could occur either at the actuation stage or at the evolution stage. Fig. 3.13 depicts the critical voltage at both the actuation stage (V_f^*) and the evolution stage (V_p^*) as a function of the electrical loading rate. It is found from Fig. 3.13, V_f^* is equal to V_p^* at low electrical loading rates. For high electrical loading rates (about over r=0.01), V_f^* becomes

higher than V_p^*. Therefore, the critical voltage at the evolution stage V_p^* should be regarded as the limiting voltage for the frequency tuning process.

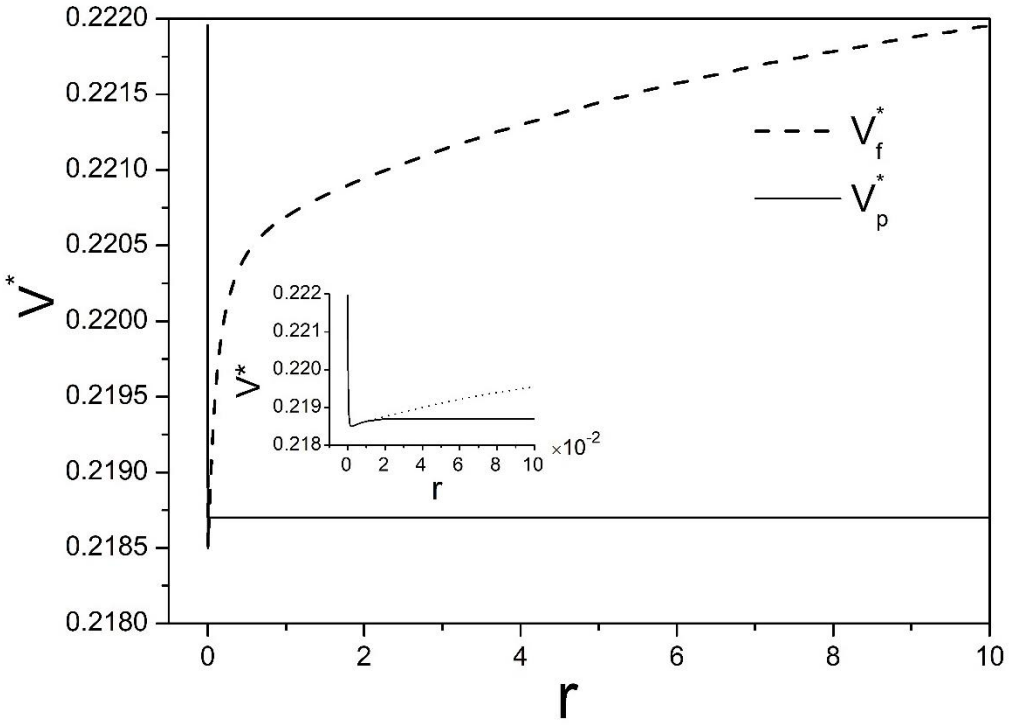

Figure 3.13 The variation of critical failure voltage with respect to the loading rate (V* Vs. r) for the DE membrane resonator with relaxation time τ =0.01 s, 1 s, 100 s, for χ =0.5, k =1, λ_{1p}=2, and λ_{2p}=4.

In Figs. 3.10(d) and 3.12, the difference of the natural frequency between the final steady state and initial steady state is defined as the frequency tuned by the applied voltage, which is denoted as $\Delta\Omega_n$. For a given geometry of the resonator, $\Delta\Omega_n$ is solely determined by the pre-set voltage, which should be selected below the critical voltage. Fig 3.14 depicts how the tuned frequency $\Delta\Omega_n$ varies with V_p^* for a DE resonator. The DE membrane is modelled with three polymer subnetworks with relaxation time τ =0.01 s, 1 s, 100 s. The voltage V_p^* is applied from 0 to the point where the membrane fails by either loss-of-tension or electrical breakdown. Fig. 3.14 also illustrates the tuneable frequency range and the safe operation voltage range of the resonator, which are essential parameters in the design and application of DE resonators. The tuneable frequency range of the resonator is defined as

the difference between the minimum tuned frequency $\Delta\Omega_n^{min}$ and the maximum tuned frequency $\Delta\Omega_n^f$, and the safe operation voltage range is between 0 and the failure voltage. It can be seen that both the tuneable frequency range and the safe operation voltage range can be changed by choosing different electrical loading rate *r*.

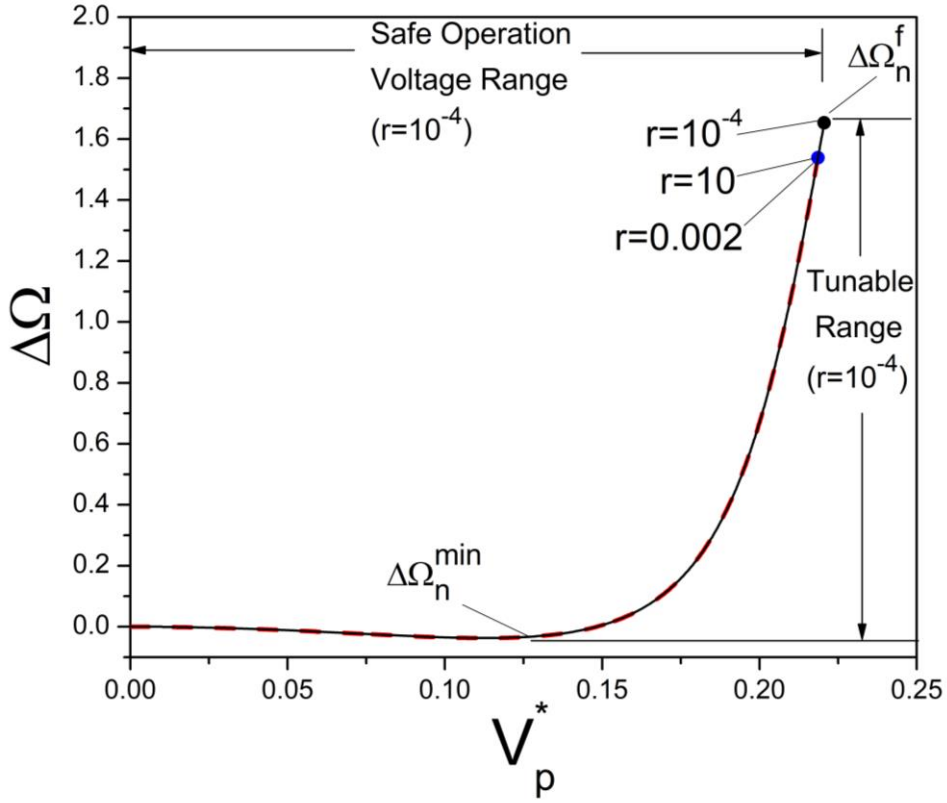

Figure 3.14 Tuneable natural frequency range and safe voltage operation range for the DE membrane resonator with relaxation time τ =0.01 s, 1 s, 100 s (n=3) for fixed parameters χ =0.5, k =1, λ_{1p}=2, λ_{2p}=4, the applied voltage is at the rate of r= 10^{-4}, 0.002, 10, respectively.

The tuneable frequency range for the viscoelastic resonator showed in Fig. 3.14 is corresponding to the prescribed material parameter (χ), geometry parameters (k, λ_{1p}, λ_{2p}) and the voltage loading rate. To account for the effect of the geometric change, Fig. 3.15 presents the variation of the tuneable frequency range of the resonator (modelled with three viscous subnetworks) as a function of the geometric parameters k, λ_{1p} and λ_{2p}. The other parameters are chosen as χ=0.5, r=0.3 and V^*=0.2. The pre-stretch ratios λ_{1p} and λ_{2p} range

from 1 to 4, respectively. The aspect ratio *k* is selected as 0.3, 1, and 2. As illustrated in Figs. 3.15(a) and 15(b) with the aspect ratio k set as 2, the frequency can be raised up to around 2.2 or brought down to -0.2. A negative value of $\Delta\Omega_n^{min}$ indicates that the membrane becomes softer after the frequency tuning process. It is observed that the maximum tuned frequency $\Delta\Omega_n^{max}$ can be significantly raised by configurating the membrane resonator with a larger aspect ratio. On the other hand, the aspect ratio only exerts a minor effect on the minimum tuned frequency $\Delta\Omega_n^{min}$. Overall, the natural frequency of the DE membrane resonator is easier to be tuned up than tuned down.

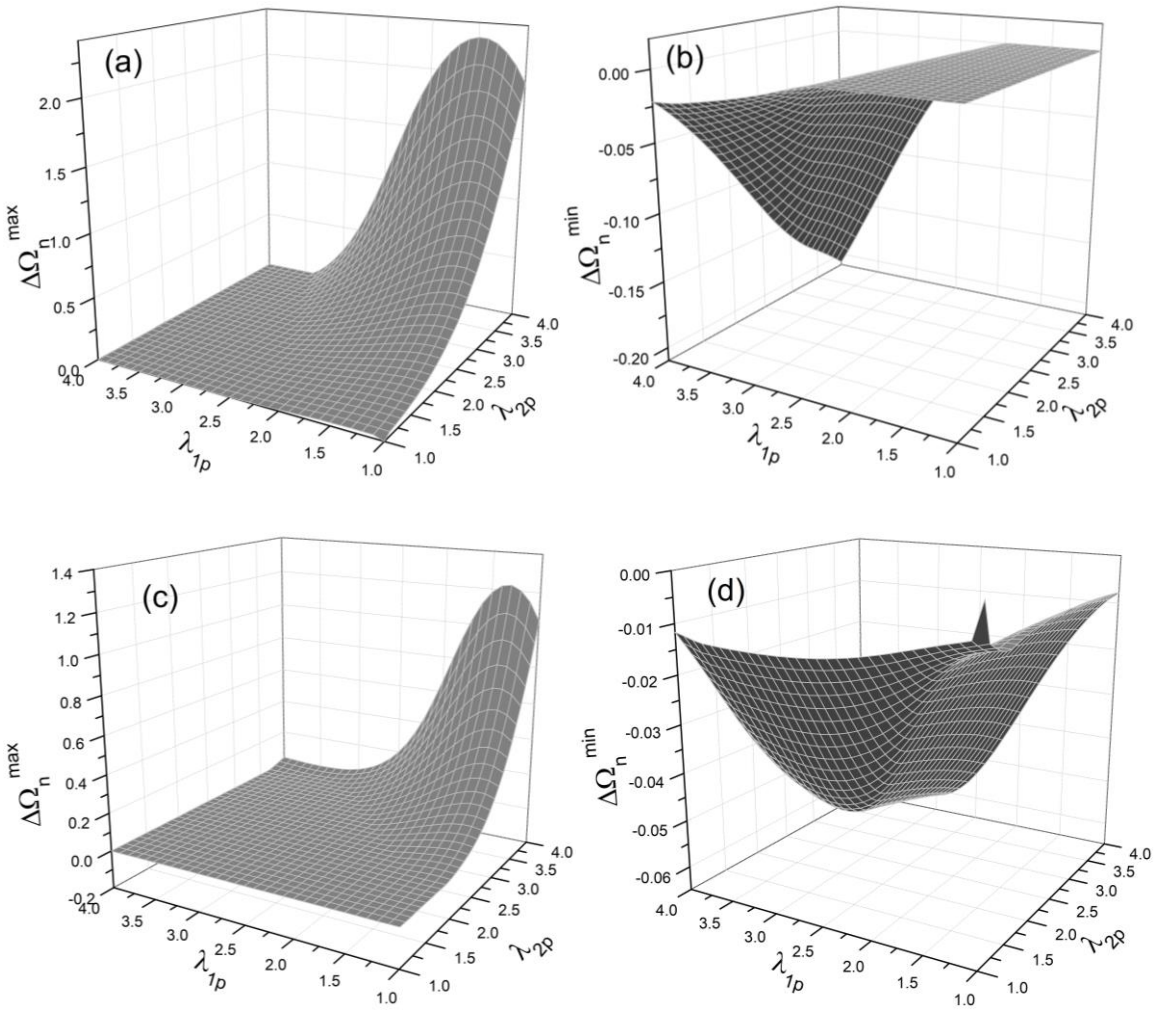

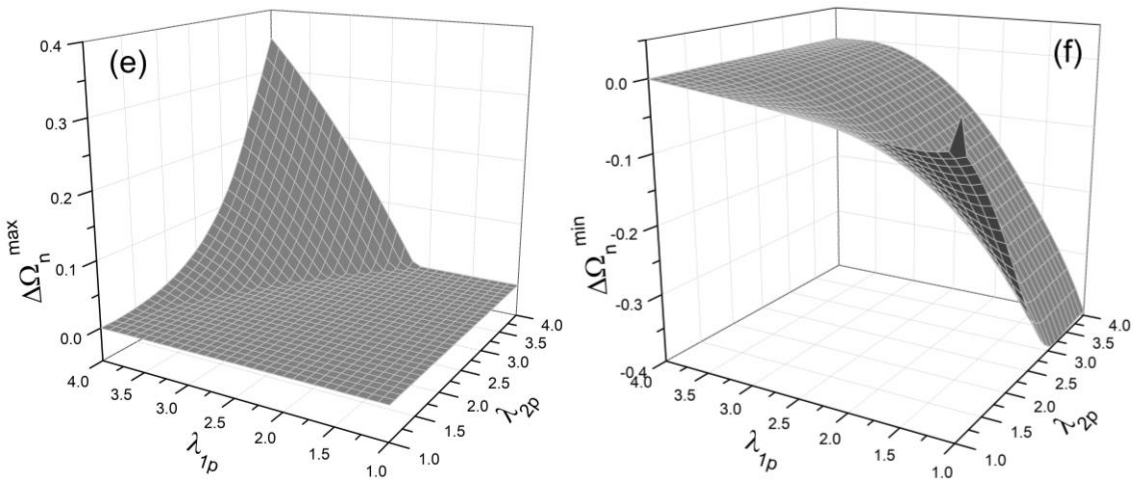

Figure 3.15 $\Delta\Omega_n^{max}$ and $\Delta\Omega_n^{min}$ of the tuneable frequency range of the viscoelastic DE memebrane resonators (χ =0.5) with relaxation time τ =0.01 s, 1 s, 100 s (n=3), for combinations of pre-stretch ratios λ_{1p} and λ_{2p}. At the actuation stage, the votage is applied at rate of r=0.3 until V^*=0.2. (a) $\Delta\Omega_n^{max}$ for *k* =2, (b) $\Delta\Omega_n^{min}$ for *k* =2, (c) $\Delta\Omega_n^{max}$ for *k* =1, (d) $\Delta\Omega_n^{min}$ for *k* =1, (e) $\Delta\Omega_n^{max}$ for *k* =0.3, (f) $\Delta\Omega_n^{min}$ for *k* =0.3.

3.5 Conclusion

The purpose of this work is to provide better understanding on the effects of material viscoelasticity with multi-relaxation on the resonant frequency tuning for DE membrane resonators. The dielectric elastomer as a polymer is simulated to be consisted of ground elastic networks and multiple viscoelastic subnetworks with different relaxation time. The viscoelastic model based on the finite deformation viscoelastic theory and Gent model of hyper-elasticity for dielectrics with one viscous subnetwork is extended to the modelling for DEs of multiple relaxation processes. The possible ways of monitoring the dynamic actuation of DE membrane resonators are proposed, by comparisons of the electromechanical responses and natural frequency variations for viscoelastic DE resonators with single or multiple (i.e. with three or two viscoelastic subnetworks) relaxation processes. The resonant frequency tuning processes of DE resonators with single or multiple viscoelastic subnetworks are presented, indicating that the ground elastic

networks govern steady states of resonators while viscoelastic subnetworks control the time to reach the steady states. Limited by failure modes of loss of tension or electric breakdown, the essential design parameters of tuneable frequency range and safe voltage operation range for DE resonators with three viscoelastic subnetworks under different electric loading rates are acquired. The tuneable frequency range within a safe voltage operation range is investigated with further consideration of various geometry parameters, suggesting that the DE membrane resonator is more favourable in vibration applications with need of natural frequency tuning-up. This work can be a reference for studying the dynamic performance of DE-based vibration devices.

Chapter 4

4 Conclusions and future work

4.1 Conclusions

As soft electroactive polymers, dielectric elastomers are featured with high flexibility and capacity of large deformation. They are desirable materials for transducers that convert mechanical and electrical energy into each other. As one of their potential applications, DE resonators and oscillators have attracted much interest in the recent years. One of the merits of DE resonators lies in their tuneable resonator frequency. While the challenging issue for DE resonators is that their dynamic performance is highly influenced by the nonlinear electromechanical coupling, the multiple failure modes and the material viscoelasticity. Aiming to comprehensively understand the dynamic behaviours of DE resonators, this work extends the widely used modelling framework for finite-deformation viscoelasticity of DEs to cover their dynamic response. Furthermore, the modelling framework is further modified to account for the multiple relaxation processes of DEs. From our simulation results, it is found that by tailoring the microstructure of the DEs, the failure (both the electrical breakdown and loss-of-tension) of the DE membrane resonator can be delayed; larger deformation can be achieved; and the resonant frequency tuning process can be improved. In addition, DE membranes with different material viscosity may achieve similar dynamic responses if the electrical loading rates are properly selected. The tuneable frequency range and safe voltage operation range for the DE resonator are also obtained with consideration of the possible failure modes (loss-of-tension and electrical breakdown). Last but not least, it is found that this design of DE membrane resonator is more effective in tuning up the resonant frequency.

4.2 Future work

The results of this work are expected to offer guidelines for the prediction and possible monitoring ways for the dynamic performance of DE-based vibrational devices. Nevertheless, since the model here is limited to idealized DEs and the configuration of the DE is rather simple, there is substantially more work to be done in the future.

The theoretical model is only focused on homogeneous deformation here. In practical applications, DEs may undergo inhomogeneous deformation, which should be further considered. Similar to other theoretical works, we adopt a constant dielectric strength in this work. However, experiments have shown that the dielectric strength is affected by many factors such as the deformation, the voltage loading rate and the temperature. Therefore, the deformation-dependent electrical breakdown of DEs should be further considered. In addition, the multiple relaxation times could affect the dielectric strength of DEs as well. Furthermore, the relaxation time of each viscous polymer subnetwork is assumed to be constant in this work. However, according to the theory of polymer dynamics, the relaxation time of the viscous subnetwork should be deformation-dependent, and its effect on the dynamic performance of DE resonators is still unknown, this could also be a topic of our future study.

References

Ahmadi, S., Gooyers, M., Soleimani, M., & Menon, C. (2013). Fabrication and electromechanical examination of a spherical dielectric elastomer actuator. Smart Materials and Structures, 22(11).

Anderson, I. A., Hale, T., Gisby, T., Inamura, T., McKay, T., O'Brien, B., Calius, E. P. (2010). A thin membrane artificial muscle rotary motor. Applied Physics A: Materials Science and Processing, 98(1), 75–83.

Arruda, E. M. and Boyce, M. C., 1993. A three-dimensional model for the large stretch behaviour of rubber elastic materials. J. Mech. Phys. Solids 41, 389-412.

Bai, Y., Jiang, Y., Chen, B., Chiang Foo, C., Zhou, Y., Xiang, F., Suo, Z. (2014). Cyclic performance of viscoelastic dielectric elastomers with solid hydrogel electrodes. Applied Physics Letters, 104(6), 1–5.

Bar-Cohen Y., Current status and infrastructure in electroactive polymer (EAP) actuators as artificial muscles reality, potential and challenges. Bellingham, WA: SPIE Press; 2004. p. 3-52.

Bergstrom, J. S. and Boyce, M. C., 1998. Constitutive modelling of the large strain time dependent behaviour of elastomers. J. Mech. Phys. Solids 46, 931–954.

Biggs, S. J., & Hitchcock, R. N. (2010). Artificial muscle actuators for haptic displays: system design to match the dynamics and tactile sensitivity of the human finger pad, (April), 76420I.

Bonwit, N., Heim, J., Rosenthal, M., Duncheon, C., & Beavers, A. (2006). Design of commercial applications of EPAM technology. Smart Structures and Materials, 616805(March 2006), 616805–616810.

Boyce, M. C., Direct comparison of the Gent and Arruda-Boyce constitutive models of rubber elasticity, Rubber Chem. Technol. 69, 781–785 (1996).

Boyce, M. C. and Arruda, E. M., 2000. Constitutive models of rubber elasticity: a review. Rubber Chem. Technol. 73, 504–523.

Cameron, C. G., Szabo, J. P., Johnstone, S., Massey, J. and Leidner, J., 2008. Linear actuation in coextruded dielectric elastomer tubes. Sens. Actuator A 147, 286–291.

Carpi, F., Salaris, C. and Rossi, D. D., 2007. Folded dielectric elastomer actuators. Smart Mater. Struct. 16, S300–305.

Carpi, F., Rossi, D. D., Kornbluh, R., Pelrine, R. and Sommer-Larsen, P., 2008. Dielectric Elastomers as Electromechanical Transducers. Elsevier, Amsterdam.

Chiang Foo, C., Jin Adrian Koh, S., Keplinger, C., Kaltseis, R., Bauer, S., & Suo, Z. (2012). Performance of dissipative dielectric elastomer generators. Journal of Applied Physics, 111(9).

Chiba, S., Waki, M., Kornbluh, R., & Pelrine, R. (2011). Current status and future prospects of power generators using dielectric elastomers. Smart Materials and Structures, 20(12).

Christensen, R. M. (1980). A Nonlinear Theory of Viscoelasticity for Application to Elastomers. Journal of Applied Mechanics, 47(4), 762.

Cohen, N., Dayal, K., & DeBotton, G. (2016). Electro elasticity of polymer networks. Journal of the Mechanics and Physics of Solids, 92, 105–126.

Díaz-Calleja, R., & Riande, E. (2013). Comments on the influence of stretching on the permittivity of dielectric elastomers. Smart Materials and Structures, 22(3).

Dorfmann, A., & Ogden, R. W. (2005). Nonlinear electro elasticity. Acta Mechanica, 174(3–4), 167–183.

Dubois, P., Rosset, S., Niklaus, M., Dadras, M., & Shea, H. (2008). Voltage control of the resonance frequency of dielectric electroactive polymer (DEAP) membranes. Journal of Microelectromechanical Systems, 17(5), 1072–1081.

Feng, C., Jiang, L. and Lau, W. M., 2011. Dynamic characteristics of a dielectric elastomer-based microbeam resonator with small vibration amplitude. J. Micromech. Microeng. 21, 095002.

Feng C., L. Yu, W. Zhang, 2013. Dynamic analysis of a dielectric elastomer-based microbeam resonator with large vibration amplitude. International Journal of Non-Linear Mechanics 65 (2014) 63–68.

Fox, J. W. and Goulbourne, N. C., 2008. On the dynamic electromechanical loading of dielectric elastomer membranes. J. Mech. Phys. Solids 56, 2669-2686.

Fox, J. W. and Goulbourne, N. C., 2009. Electric field-induced surface transformations and experimental dynamic characteristics of dielectric elastomer membranes. J. Mech. Phys. Solids 57, 1417-1436.

Gent, A. N., 1996. A new constitutive relation for rubber. Rubber Chem. Technol. 69, 59-61.

Gerhard A. Holzapfel, 2000. Nonlinear Solid Mechanics: A Continuum Approach for Engineering. Technical University Graz, Austria. JOHN WILEY & SONS, LTD. 282-288.

Goulbourne, N., Mockensturm, E., & Frecker, M. (2005). A Nonlinear Model for Dielectric Elastomer Membranes. Journal of Applied Mechanics, 72(6), 899.

Goulbourne, N.C., Mockensturm, E. and Frecker, M.I. 2007. Electro-elastomers: Large Deformation Analysis of Silicone Membranes. International Journal of Solids and Structures, 44:2609_2626.

Guo, J., Xiao, R., Park, H. S., & Nguyen, T. D. (2015). The Temperature-Dependent Viscoelastic Behaviour of Dielectric Elastomers. Journal of Applied Mechanics, 82(9), 091009.

G. Yang, G. Yao, W. Ren, G. Akhras, J.P. Szabo and B.K. Mukherjee. 2005. The strain response of silicone dielectric elastomer actuators. Smart Structures and Materials: Electroactive Polymer Actuators and Devices, SPIE Proc.5759, 134-143.

Heydt, R., Kornbluh, R., Eckerle, J., & Pelrine, R. (2006). Sound radiation properties of dielectric elastomer electroactive polymer loudspeakers, (March 2006), 61681M.

Hong, W. (2011). Modelling viscoelastic dielectrics. Journal of the Mechanics and Physics of Solids, 59(3), 637–650.

Hossain, M., Vu, D. K., & Steinmann, P. (2012). Experimental study and numerical modelling of VHB 4910 polymer. Computational Materials Science, 59, 65–74.

Hossain, M., Vu, D. K., & Steinmann, P. (2015). A comprehensive characterization of the electro-mechanically coupled properties of VHB 4910 polymer. Archive of Applied Mechanics, 85(4), 523–537.

Huang, J., Shian, S., Diebold, R. M., Suo, Z., & Clarke, D. R. (2012). The thickness and stretch dependence of the electrical breakdown strength of an acrylic dielectric elastomer. Applied Physics Letters, 101(12).

Huang, J., Lu, T., Zhu, J., Clarke, D. R. and Suo, Z., 2012b. Large, uni-directional actuation in dielectric elastomers achieved by fiber stiffening. Appl. Phys. Lett. 100, 211901.

Huang, J., Shian, S., Suo, Z., & Clarke, D. R. (2013). Dielectric elastomer generator with equi-biaxial mechanical loading for energy harvesting, 86870Q.

Huang, R. and Suo, Z., 2011. Electromechanical phase transition in dielectric elastomers. Proc. R. Soc. A 468, 1014–1040.

Khan, K.A., Wafai, H., El Sayed, T., 2013. A variational constitutive framework for the nonlinear viscoelastic response of a dielectric elastomer. Comput. Mech. 52, 345-360.

Karsten, R., Flittner, K., Haus, H., & Schlaak, H. F. (2013). Development of an active isolation mat based on dielectric elastomer stack actuators for mechanical vibration cancellation, (April 2013), 86870Y.

Kofod, G., Sommer-Larsen, P., Kornbluh, R., & Pelrine, R. (2003). Actuation response of polyacrylate dielectric elastomers. Journal of Intelligent Material Systems and Structures, 14(12), 787–793.

Koh, S. J. A., Li, T., Zhou, J., Zhao, X., Hong, W., Zhu, J., & Suo, Z. (2011). Mechanisms of large actuation strain in dielectric elastomers. Journal of Polymer Science, Part B: Polymer Physics, 49(7), 504–515.

Kollosche, M., Kofod, G., Suo, Z., & Zhu, J. (2015). Temporal evolution and instability in a viscoelastic dielectric elastomer. Journal of the Mechanics and Physics of Solids, 76, 47–64.

Kollosche, M., Zhu, J., Suo, Z., & Kofod, G. (2012). Complex interplay of nonlinear processes in dielectric elastomers. Physical Review E - Statistical, Nonlinear, and Soft Matter Physics, 85(5), 2–5.

Kornbluh, R., Pelrine, R., Joseph, J, Heydt, R., Pei, Q. and Chiba, S., 1999. High-field electrostriction of elastomeric polymer dielectrics for actuation. Proc. SPIE 3669, 149-161.

Kornbluh, R., Pelrine, R., Pei, Q., Heydt, R., Stanford, S., Oh, S. and Eckerle, J., 2002. Electro elastomers: applications of dielectric elastomer transducers for actuation, generation and smart structures. Proc. SPIE 4698, 254 - 270.

Kornbluh, R. D., Pelrine, R., Pei, Q., Oh, S., & Joseph, J. (2000). Ultrahigh strain response of field-actuated elastomeric polymers, (June 2000), 51.

Lai, W., Bastawros, A. F., & Hong, W. (2012). Out-of-Plane Motion of a Planar Dielectric Elastomer Actuator with Distributed Stiffeners. Electroactive Polymer Actuators and Devices, 8340, 834011-834011–834017.

Lee, E. H., 1969, Elastic-Plastic Deformation at Finite Strains". ASME J. Appl. Mech., 36, pp. 1–6.

Li, T., Qu, S., & Yang, W. (2012). Electromechanical and dynamic analyses of tuneable dielectric elastomer resonator. International Journal of Solids and Structures, 49(26), 3754–3761.

Li, Y., Tang, S., Kröger, M., & Liu, W. K. (2016). Molecular simulation guided constitutive modelling on finite strain viscoelasticity of elastomers. Journal of the Mechanics and Physics of Solids, 88, 204–226.

Linder, C., Tkachuk, M., & Miehe, C. (2011). A micromechanically motivated diffusion-based transient network model and its incorporation into finite rubber viscoelasticity. Journal of the Mechanics and Physics of Solids, 59(10), 2134–2156.

Liu, L., Sun, W., Sheng, J., Chang, L., Li, D., & Chen, H. (2015). Effect of temperature on the electromechanical actuation of viscoelastic dielectric elastomers. Epl, 112(2), 1–5.

Lu, T., Huang, J., Jordi, C., Kovacs, G., Huang, R., Clarke, D. R. and Suo, Z., 2012. Dielectric elastomer actuators under equal-biaxial forces, uniaxial forces, and uniaxial constraint of stiff fibres. Soft Matter 8, 6167–6173.

McMeeking, R. M., & Landis, C. M. (2005). Electrostatic Forces and Stored Energy for Deformable Dielectric Materials. Journal of Applied Mechanics, 72(4), 581.

Michel, S., Zhang, X. Q., Wissler, M., Löwe, C., & Kovacs, G. (2010). A comparison between silicone and acrylic elastomers as dielectric materials in electroactive polymer actuators. Polymer International, 59(3), 391–399.

McKay, T., O'Brien, B., Calius, E. and Anderson, I., 2010. An integrated, self-priming dielectric elastomer generator. Appl. Phys. Lett. 97, 062911.

Mockensturm, E. M. and Goulbourne, N., 2006. Dynamic response of dielectric elastomers. Int. J. Nonlinear Mech. 41, 388-395.

Mooney, M., 1940. A theory of large elastic deformation. J. Appl. Phys. 11, 582-592.

O’Brien, B. M., Calius, E. P., Inamura, T., Xie, S. Q., & Anderson, I. A. (2010). Dielectric elastomer switches for smart artificial muscles. Applied Physics A: Materials Science and Processing, 100(2), 385–389.

O’Brien, B. M., Rosset, S., Shea, H. R., & Anderson, I. A. (2012). Cutting the fat: artificial muscle oscillators for lighter, cheaper, and slimmer devices, 8340, 834008.

Ogden, R. W., 1972. Large deformation isotropic elasticity-on the correlation of theory and experiment for incompressible rubberlike solids. Proc. R. Soc. Lond. A. 326, 565-584.

O’Halloran, A., O’Malley, F., & McHugh, P. (2008). A review on dielectric elastomer actuators, technology, applications, and challenges. Journal of Applied Physics, 104(7).

Park, H. S., & Nguyen, T. D. (2013). Viscoelastic effects on electromechanical instabilities in dielectric elastomers. Soft Matter, 9(4), 1031–1042.

Park, H. S., Suo, Z., Zhou, J., & Klein, P. A. (2012). A dynamic finite element method for inhomogeneous deformation and electromechanical instability of dielectric elastomer transducers. International Journal of Solids and Structures, 49(15–16), 2187–2194.

Pei, Q., Rosenthal, M., Stanford, S., Prahlad, H. and Pelrine, R., 2004. Multiple-degrees of-freedom electro elastomer roll actuators. Smart Mater. Struct. 13, N86–92.

Pelrine, R. E., Kornbluh, R. D. and Joseph, J. P., 1998. Electrostriction of polymer dielectrics with compliant electrodes as a means of actuation. Sens. Actuators A 64, 77-85.

Pelrine, R., Kornbluh, R., Pei, Q., & Joseph, J. (2000). High-speed electrically actuated elastomers with strain greater than 100%. Science, 287(5454), 836–839.

Pelrine, R., Kornbluh, R.D., Pei, Q., Stanford, S., Oh, S., Eckerle, J., Full, R., Rosenthal, M. and Meijer, K., 2002. Dielectric elastomer artificial muscle actuators: toward biomimetic motion. Proc. SPIE 4695, 126-137.

Plante, J. S., & Dubowsky, S. (2006). Large-scale failure modes of dielectric elastomer actuators. International Journal of Solids and Structures, 43(25–26), 7727–7751.

Plante, J. S., & Dubowsky, S. (2007). On the performance mechanisms of Dielectric Elastomer Actuators. Sensors and Actuators, A: Physical, 137(1), 96–109.

Reese, S., & Govindjee, S. (1998). A theory of finite viscoelasticity and numerical aspects. International Journal of Solids and Structures, 35(26–27), 3455–3482.

Rivlin, R. S., 1948. Large elastic deformations of isotropic materials. IV. Further developments of the general theory. Philos. Trans. R. Soc. London. Ser. A 241, 379-397.

Romasanta, L. J., Lopez-Manchado, M. A., & Verdejo, R. (2015). Increasing the performance of dielectric elastomer actuators: A review from the materials perspective. Progress in Polymer Science, 51(September), 188–211.

R. Zhang, P Iravani and P S Keogh, 2018. Modelling dielectric elastomer actuators using higher order material characteristics. J. Phys. Commun. 2 (2018) 045025.

Saito, Y., Takao, H., Tani, T., Nonoyama, T., Takatori, K., Homma, T., Nagaya, T. and Nakamura M., 2004. Lead-free piezoceramics. Nature 432, 84-87.

Shankar, R., Ghosh, T. K., & Spontak, R. J. (2007). Dielectric elastomers as next-generation polymeric actuators. Soft Matter, 3(9), 1116.

Shian, S., Huang, J., Zhu, S., & Clarke, D. R. (2014). Optimizing the Electrical Energy Conversion Cycle of Dielectric Elastomer Generators. Advanced Materials, 26(38), 6617–6621.

Shmuel, G., & Pernas-Salomïn, R. (2016). Manipulating motions of elastomer films by electrostatically-controlled aperiodicity. Smart Materials and Structures, 25(12), 1–13.

Son, S., & Goulbourne, N. C. (2010). Dynamic response of tubular dielectric elastomer transducers. International Journal of Solids and Structures, 47(20), 2672–2679.

Suo, Z. (2010). Theory of dielectric elastomers. Acta Mechanica Solida Sinica, 23(6), 549–578.

Suo, Z., Zhao, X., & Greene, W. H. (2008). A nonlinear field theory of deformable dielectrics. Journal of the Mechanics and Physics of Solids, 56(2), 467–486.

Tagarielli, V. L., Hildick-Smith, R., & Huber, J. E. (2012). Electro-mechanical properties and electrostriction response of a rubbery polymer for EAP applications. International Journal of Solids and Structures, 49(23–24), 3409–3415.

Treloar, L. R. G., 1944. Stress-strain data for vulcanised rubber under various types of deformation. Trans. Faraday Soc. 40, 59-70.

Vogel V., Goktepe, S., Steinmann, P., Kuhl, E., 2014. Modelling and simulation of viscous electro-active polymers. Eur. J. Mech. A/Solids 48,112-128.

Wang, H., Lei, M., & Cai, S. (2013). Viscoelastic deformation of a dielectric elastomer membrane subject to electromechanical loads. Journal of Applied Physics, 113(21), 1–7.

Wang, J., Nguyen, T. D., & Park, H. S. (2013). Electrostatically Driven Creep in Viscoelastic Dielectric Elastomers. Journal of Applied Mechanics, 81(5), 051006.

Wang, S., Decker, M., Henann, D. L., & Chester, S. A. (2016). Modelling of dielectric viscoelastomers with application to electromechanical instabilities. Journal of the Mechanics and Physics of Solids, 95, 213–229.

Wissler, M., & Mazza, E. (2005a). Modelling and simulation of dielectric elastomer actuators. Smart Materials and Structures, 14(6), 1396–1402.

Wissler, M., & Mazza, E. (2005b). Modelling of a pre-strained circular actuator made of dielectric elastomers. Sensors and Actuators, A: Physical, 120(1), 184–192.

Wissler, M., & Mazza, E. (2007). Mechanical behaviour of an acrylic elastomer used in dielectric elastomer actuators. Sensors and Actuators, A: Physical, 134(2), 494–504.

W. Ma and L. Cross, (2004). An experimental investigation of electromechanical response in a dielectric acrylic elastomer," Appl. Phys. A: Mater. Sci. Process. 78, 1201–1204.

Xiao, R. (2016). Modelling shape-memory behaviour of dielectric elastomers. Epl, 114(1).

Yang, E., Frecker, M., & Mockensturm, E. (2005). Viscoelastic model of dielectric elastomer membranes, (May 2005), 82.

Yeoh, O. H., 1993. Some forms of the strain energy function for rubber. Rubber Chem. Technol. 66, 754-771.

Yong, H., He, X. and Zhou, Y., 2011. Dynamics of a thick-walled dielectric elastomer spherical shell. Int. J. Eng. Sci. 49, 792-800.

Zhang, G., Gaspar, J., Chu, V., & Conde, J. P. (2005). Electrostatically actuated polymer microresonators. Applied Physics Letters, 87(10), 1–4.

Zhang, J., Chen, H., Sheng, J., Liu, L., Wang, Y., & Jia, S. (2014a). Dynamic performance of dissipative dielectric elastomers under alternating mechanical load. Applied Physics A: Materials Science and Processing, 116(1), 59–67.

Zhang J., Hualing Chen (2014b) Electromechanical performance of a viscoelastic dielectric elastomer balloon, International Journal of Smart and Nano Materials, 5:2, 76-85, DOI: 10.1080/19475411.2014.893930.

Zhang, J., Tang, L., Li, B., Wang, Y., & Chen, H. (2015). Modelling of the dynamic characteristic of viscoelastic dielectric elastomer actuators subject to different conditions of mechanical load. Journal of Applied Physics, 117(8).

Zhang, J., Zhao, J., Chen, H., & Li, D. (2017a). Dynamic analyses of viscoelastic dielectric elastomers incorporating viscous damping effect. Smart Materials and Structures, 26(1).

Zhang J, Wang Y, McCoul D., Pei Q. and Chen H. 2014. Viscoelastic creep elimination in dielectric elastomer actuation by preprogrammed voltage. Applied Physics Letters 105 212904.

Zhang J, Ru J, Chen H., Li D. and Lu J. 2017b. Viscoelastic creep and relaxation of dielectric elastomers characterized by a Kelvin-Voigt-Maxwell model. Applied Physics Letters 110 044104.

Zhang J, Chen H. and Li D. 2017c. Nonlinear dynamical model of a soft viscoelastic dielectric elastomer. Physical Review Applied 8 064016.

Zhang, X., Wissler, M., Jaehne, B., Breonnimann, R., & Kovacs, G. (2004). Effects of crosslinking, prestrain, and dielectric filler on the electromechanical response of a new silicone and comparison with acrylic elastomer, (July 2004), 78.

Zhao, X., Hong, W., & Suo, Z. (2007). Electromechanical hysteresis and coexistent states in dielectric elastomers. Physical Review B - Condensed Matter and Materials Physics, 76(13), 1–9.

Zhao X, Koh S, Suo Z (2011) Nonequilibrium thermodynamics of dielectric elastomers. Int J Appl Mech 3:203–217.

Zhao, X. and Suo, Z., 2007. Method to analyse electromechanical stability of dielectric elastomers. Appl. Phys. Lett. 91, 061921.

Zhao, X. and Suo, Z. 2008. Electrostriction in elastic dielectrics undergoing large deformation. J. Appl. Phys. 104, 123530.

Zhao, X. and Suo, Z., 2010. Theory of dielectric elastomers capable of giant deformation of actuation. Phys. Rev. Lett. 104, 178302.

Zhou, J. (2015a). Electromechanical coupling behaviour of dielectric elastomer transducers, (September).

Zhou, J., Jiang, L., & Khayat, R. E. (2013). Failure analysis of a dielectric elastomer plate actuator considering boundary constraints. Journal of Intelligent Material Systems and Structures, 24(14), 1667–1674.

Zhou, J., Jiang, L., & Khayat, R. E. (2014). Viscoelastic effects on frequency tuning of a dielectric elastomer membrane resonator. Journal of Applied Physics, 115(12).

Zhou, J., Jiang, L., & Khayat, R. E. (2015b). Investigation on the performance of a viscoelastic dielectric elastomer membrane generator. Soft Matter, 11(15), 2983–2992.

Zhou, J., Jiang, L., & Khayat, R. (2016a). Analysis on the energy harvesting cycle of dielectric elastomer generators for performance improvement. Epl, 115(2).

Zhou, J., Jiang, L., & Khayat, R. E. (2016b). Dynamic analysis of a tuneable viscoelastic dielectric elastomer oscillator under external excitation. Smart Materials and Structures, 25(2), 25005.

Zhou, J., Jiang, L., & Khayat, R. E. (2017). Methods to improve harvested energy and conversion efficiency of viscoelastic dielectric elastomer generators. Journal of Applied Physics, 121(18).

Zhou, J., Jiang, L., & Khayat, R. E. (2018). A micro–macro constitutive model for finite deformation viscoelasticity of elastomers with nonlinear viscosity. Journal of the Mechanics and Physics of Solids, 110, 137–154.

Zhu, J., Cai, S. and Suo, Z., 2010a. Resonant behaviour of a membrane of a dielectric elastomer. Int. J. Solids Struct. 47, 3254-3262.

Zhu, J., Cai, S. and Suo, Z., 2010b. Nonlinear oscillation of a dielectric elastomer balloon. Polym. Int. 59, 378-383.

Zhu, J., Stoyanov, H., Kofod, G. and Suo, Z., 2010c. Large deformation and electromechanical instability of a dielectric elastomer tube actuator. J. Appl. Phys. 108, 074113.

Curriculum Vitae

Name:	Liyang Tian
Post-secondary Education and Degrees:	Central South University Changsha, Hunan, China 2006-2010 B.A. Central South University Changsha, Hunan, China 2010-2013 M.A. The University of Western Ontario London, Ontario, Canada 2015-2018 M.A.
Related Work Experience	Teaching Assistant The University of Western Ontario 2015-2017